

AD-A040 915

UTAH STATE UNIV LOGAN ELECTRO-DYNAMICS LAB
COMPUTER-AIDED ESTIMATES OF THE ROTATIONAL TEMPERATURES OF O₂ I--ETC(U)
JUL 76 S SUE, D J BAKER
SCIENTIFIC-5

F/G 7/4

F19628-73-C-0048

AFGL-TR-76-0212

NL

UNCLASSIFIED

1 OF 1
ADA040915



END

DATE
FILMED

7-77

AD A 040915

AFGL-TR-76-0212

COMPUTER-AIDED ESTIMATES OF THE ROTATIONAL
TEMPERATURES OF O₂ IN THE MESOSPHERE

Shou-Chi Sue and Doran J. Baker

Electro-Dynamics Laboratories
Utah State University
Logan, Utah 84322

July 1976

Scientific Report No. 5

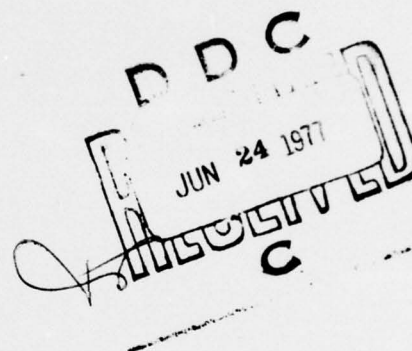
Approved for public release, distribution unlimited

This research was sponsored by the Defense Nuclear
Agency under Subtask L25AAXHX966, Work Unit 32, entitled:
"Infrared Instrument Development and Certification."

Prepared for

AIR FORCE GEOPHYSICS LABORATORY
AIR FORCE SYSTEMS COMMAND
UNITED STATE AIR FORCE
HANSCOM AFB, MASSACHUSETTS 01731

AD No. _____
DDC FILE COPY



Qualified requestors may obtain additional copies from the Defense Documentation Center. All others should apply to the National Technical Information Service.

UNCLASSIFIED

SECURITY CLASSIFICATION OF THIS PAGE (When Data Entered)

| 19 REPORT DOCUMENTATION PAGE | | READ INSTRUCTIONS BEFORE COMPLETING FORM | |
|--|---|---|---|
| 18 REFERENCE NUMBER | 2 DEVT ACCESSION NO | 3 RECIPIENT'S CATALOG NUMBER | |
| 4 TITLE (and Subtitle) | 5 PERFORMING ORG. REPORT NUMBER | | 14 |
| 6 COMPUTER-AIDED ESTIMATES OF THE ROTATIONAL TEMPERATURES OF O_2^+ IN THE MESOSPHERE, | 7 AUTHOR | | Scientific Report No. 5 |
| 8 AUTHOR | 9 PERFORMING ORGANIZATION NAME AND ADDRESS | | 10 CONTRACT OR GRANT NUMBER |
| 10 Shou-Chi/Sue and Doran J./Baker | Electro-Dynamics Laboratories Utah State University Logan, Utah 84322 123 870 | | F19628-73-C-9948 |
| 11 CONTROLLING OFFICE NAME AND ADDRESS | 12 REPORT DATE | | 13 PROGRAM ELEMENT PROJECT TASK AREA & WORK UNIT NUMBER |
| Air Force Geophysics Laboratory Hanscom AFB, Massachusetts 01731 Monitor/ A.T. Stair/ OPR | July 1976 | | CDNA0012 |
| 14 MONITORING AGENCY NAME & ADDRESS (if different from Controlling Office) | 15 SECURITY CLASS. OF THIS REPORT | | 16 DISTRIBUTION STATEMENT (of this Report) |
| 123 p. | Unclassified | | Approved for public release; distribution unlimited |
| 17 DISTRIBUTION STATEMENT (of the abstract entered in Block 20, if different from Report) | | | |
| 18 SUPPLEMENTARY NOTES | | | |
| This research was sponsored by the Defense Nuclear Agency under Subtask L25AAXHX966, Work Unit 32, entitled: "Infrared Instrument Development and Certification." | | | |
| 19 KEY WORDS (Continue on reverse side if necessary, and identify by block number) | | | |
| Temperature, rotational temperature, atmosphere, mesosphere, oxygen, infrared, airglow. $(b(1) \text{ Sigma}(g, +))$ | | | |
| 20 ABSTRACT (Continue on reverse side if necessary, and identify by block number) | | | |
| Measurements have been made of the apparent rotational temperature of $O_2(b^1\Sigma_g^+)$ atmospheric (0,1) band emissions. The data were taken at nighttime in the auroral zone at Poker Flat, Alaska, on March 1, 1975. The average apparent temperature was 210° K and the zenith radiance of the band was 500 R (uncorrected for atmospheric extinction). A comparison technique was developed to compare the | | | |

DD FORM 1 JAN 73 1473 EDITION OF 1 NOV 65 IS OBSOLETE

UNCLASSIFIED

SECURITY CLASSIFICATION OF THIS PAGE (When Data Entered)

→ next page

123 870

LB

UNCLASSIFIED

SECURITY CLASSIFICATION OF THIS PAGE (When Data Entered)

20. (Continued)

cont

→ band shape of the measured band with theoretical spectra synthesized at different, but specific, rotational temperatures. Three methods of comparison were used and it was concluded that a sum of squares weighting approach is near optimal for estimating rotational temperatures. The effect of noise was tested by adding real typical noise to the synthetic model. The same comparison technique was then applied to assess the benefits of noise. The uncertainty of the measurement is estimated to be $\pm 5^\circ\text{K}$. A "wavelike" fluctuation of the apparent rotational temperature, with a period on the order of 1/2 to 1 hour, was observed. The fluctuation on this occasion appeared to covary with the intensity of the OH airglow emission.

↑

SECURITY CLASSIFICATION OF THIS PAGE (When Data Entered)

LIST OF CONTRIBUTORS

Doran J. Baker - Principal Investigator

U. Ralph Embry
William R. Pendleton
Allan J. Steed
Gene A. Ware

ACKNOWLEDGMENTS

The success of this experimental program was made possible through the combined efforts of numerous members of the staffs of the Defense Nuclear Agency (program sponsors), the Air Force Geophysics Laboratory, the University of Alaska, Utah State University, and many others participated in the ICECAP '75 measurements program at Poker Flat, Alaska. These contributions are gratefully acknowledged. The efforts of Dr. A.T. Stair, Jr., and Mr. J.C. Ulwick (both of AFGL), Dr. K.D. Baker, Mr. A.J. Steed, Mr. G.A. Ware, Mr. U.R. Embry and Dr. W.R. Pendleton (all of USU) on behalf of the project are specifically acknowledged.

| | |
|---------------------------------|---|
| ACCESSION FOR | |
| RVIS | Write Section <input checked="" type="checkbox"/> |
| DOC | Ref Section <input type="checkbox"/> |
| UNANNOUNCED | <input type="checkbox"/> |
| JUSTIFICATION | |
| BY | |
| DISTRIBUTION AVAILABILITY CODES | |
| Dist | Avail and/or Special |
| A | |

TABLE OF CONTENTS

| | Page |
|--|------|
| LIST OF CONTRIBUTORS AND ACKNOWLEDGMENTS | iii |
| RELATED CONTRACTS | iii |
| LIST OF TABLES | vii |
| LIST OF FIGURES | ix |
| INTRODUCTION | 1 |
| Background | 1 |
| Emission Mechanisms | 6 |
| OBJECTIVES | 11 |
| SYNTHETIC SPECTRUM | 13 |
| Line Spectrum | 13 |
| Synthetic Spectrum | 14 |
| INSTRUMENT DESCRIPTION | 21 |
| SPECTRAL COMPARISON METHOD | 25 |
| Comparison Technique | 25 |
| Recommendations. | 30 |
| CONCLUSIONS AND RECOMMENDATIONS | 39 |
| Conclusions | 39 |
| Recommendations | 39 |
| REFERENCES | 41 |
| APPENDIX A - Notation of Energy State of Molecule | A-1 |
| APPENDIX B - Relative Abundance of $O_2(X^3\Sigma_g^-, v=1)$, with Respect to Temperature. | B-1 |
| APPENDIX C - Theoretical Review | C-1 |
| Vibrating Rotator Model | C-1 |

TABLE OF CONTENTS (cont.)

| | |
|---|-----|
| Hund's Coupling | C-1 |
| Transitions of $O_2(b^1\Sigma_g^- \rightarrow X^3\Sigma_g^-)$ | C-5 |
| APPENDIX D - List of Computer Programs | D-1 |
| APPENDIX E - Values of Instrumental Response | E-1 |
| APPENDIX F - Measured Zenith Emission Rates of $O_2(b^1\Sigma_g^-)$ Atmospheric (0,1) Band | F-1 |
| APPENDIX G - Measured Spectrum of $O_2(b^1\Sigma_g^+)$ Atmospheric (0,1) Band at Poker Flat on March 1, 1975 | G-1 |
| APPENDIX H - Distribution List | H-1 |

LIST OF TABLES

| Table | Page |
|--|------|
| 1. Daytime atmospheric airglow species | 2 |
| 2. Band systems and wavelengths of transitions of O_2 | 3 |
| 3. The band systems of O_2 in the airglow spectrum | 4 |
| 4. O_2 atmospheric band radiances under auroral conditions | 4 |
| 5. Rotational temperatures of $O_2(b^1\Sigma_g^+)$ (0,1) band calculated using three approaches | 32 |
| 6. Rotational temperatures computed from $O_2(b^1\Sigma_g^+)$ atmospheric (0,1) band at 8645 Å | 36 |
| C.1. Rotational constants of the $X^3\Sigma_g^-$ and $b^1\Sigma_g^+$ states of O_2 | C-6 |
| C.2. Wavenumbers (cm^{-1}) of lines in (0-1) band of $O_2(^1\Sigma - ^3\Sigma)$ | C-9 |

LIST OF FIGURES

| Figure | Page |
|---|------|
| 1. Simplified energy levels and transitions of O_2 | 5 |
| 2. Typical average altitude profiles for $[O_2]$, $[O_3]$ and temperature for winter conditions at 60° latitude | 8 |
| 3. $O_2(b^1\Sigma_g^+)$ atmospheric (0,1) band synthetic line spectrum at $T = 210^\circ K$ | 15 |
| 4. The synthetic spectrum of $O_2(b^1\Sigma_g^+)$ atmospheric (0,1) band with 3.0 cm^{-1} resolution | 17 |
| 5. The synthetic spectrum of $O_2(b^1\Sigma_g^+)$ atmospheric (0,1) band with 4.34 cm^{-1} resolution | 18 |
| 6. Theoretical spectra of $O_2(b^1\Sigma_g^+)$ atmospheric (0,1) band at different temperatures | 19 |
| 7. A simplified schematic diagram of the EDL interferometer-spectrometer system | 22 |
| 8. The night airglow spectrum of $O_2(b^1\Sigma_g^+)$ atmospheric (0,1) band measured at Poker Flat, Alaska at 8:45 hrs. UT($\lambda=121^\circ$) on March 1, 1975 | 26 |
| 9. The relative intensity of sunlight and the instrument response with respect to sunlight | 27 |
| 10. The normalized total response with respect to wavenumber over the range of $O_2(b^1\Sigma_g^+)$ atmospheric (0,1) band | 29 |
| 11. Comparison of theoretical models of different temperatures and measured spectrum | 31 |
| 12. Apparent rotational temperature of $O_2(b^1\Sigma_g^+)$ atmospheric (0,1) band of each scan | 33 |
| 13. Theoretical volume emission rates for the $O_2(b^1\Sigma_g^+)$ atmospheric (0,1) band night airglow | 35 |
| 14. Day airglow volume emission rates profile of the $O_2(b^1\Sigma_g^+)$ atmospheric (0,1) band from rocket borne photometer | 35 |

LIST OF FIGURES (cont.)

| Figure | Page |
|---|------|
| 15. Apparent correlation between the rotational temperature of $O_2(b^1\Sigma_g^+)$ atmospheric (0,1) band and the zenith radiance of the OH(5,3) band observed above Poker Flat, Alaska on March 1, 1975 | 37 |
| C.1. The vector diagram of Hund's case (b) | C-4 |
| C.2. Transition between $b^1\Sigma_g^+$ and $X^3\Sigma_g^-$ | C-8 |
| F.1. The observation of zenith emission of $O_2(b^1\Sigma_g^+)$ atmospheric (0,1) band from rocket | F-1 |
| F.2. Zenith emission rates observed by rocket borne photometer and spectrometer | F-1 |
| G.1. Coadded (T) spectrum $O_2(b^1\Sigma_g^+)$ atmospheric (0,1) band obtained from zenith observations at Poker Flat, Alaska at 0831-0834 hrs. UT, on March 1, 1975 | G-1 |

INTRODUCTION

Background

Many atomic and molecular species contribute to the radiation from the upper atmosphere. A partial list of the observed day airglow radiations, made at high altitude, is shown in Table 1. Most of these cannot be observed at the surface of the earth, because the intensity of scattered sunlight is much greater.

During twilight and nighttime, surface observation of the emission from several upper-atmospheric airglow species is possible. Of particular interest here is the radiation from excited oxygen molecules. The atmospheric band system of O_2 , $b^1\Sigma_g^+ \rightarrow X^3\Sigma_g^-$, was first discovered by *Meinel* [1950,1951] in the airglow and later in aurora. (For molecular state symbolism see Appendix A).

The spectra of atmospheric and infrared atmospheric bands of O_2 are now well established as features of the airglow spectrum. A detailed listing of the band systems for known transitions of O_2 is given in Table 2. Table 3 gives the observed radiances for the Herzberg bands and two bands of the atmospheric and infrared atmospheric band systems, all taken at high altitude using balloon-borne equipment.

Figure 1 shows a simplified energy level diagram for the oxygen molecule, with two vibrational levels corresponding to $v=0$, and $v=1$. The (0,0) band at 7600 Å and the (0,1) band at 8645 Å correspond to the transitions from the state ($b^1\Sigma_g^+$, $v=0$) to the states ($X^3\Sigma_g^-$, $v=0$) and ($X^3\Sigma_g^-$, $v=1$), respectively. According to the airglow radiances of Table 3, and the auroral radiances given in Table 4, the radiance of the (0,0) band is typically about 20 times that of the (0,1) band. In ground-based observations, the (0,0) band is completely reabsorbed by the great amount of O_2 in the ground state ($X^3\Sigma_g^-$, $v=0$) in the lower atmosphere. The low concentration of O_2 molecules in the vibrationally-excited state ($X^3\Sigma_g^-$, $v=1$) causes little absorption of the (0,1) band.

Table 1. Daytime atmospheric airglow species [Whitten and Poppoff, 1971].

| Emission | Wavelength (Å or μm) | Zenith Radiance (kR) |
|--|-------------------------------------|-------------------------|
| Lyman α | 1216 | 5-12 |
| OI($^3P-^3S$) | 1304 | 2-6 |
| OI($^3P-^5S$) | 1355 | 0.4 |
| NO(ν) | 2000-3000 | 1 |
| N (2PG) | 3000-4000 | 0.4 |
| N $_2^+$ (1N) | 3914 | 2-7 |
| NI($^4S-^2D$) | 5200 | 0.1 |
| OI($^1D-^1S$) | 5577 | 0.4-3 |
| Na(D) | 5893 | 2-40 |
| OI($^3P-^1D$) | 6300 | 3-60 |
| O $_2$ ($b^1\Sigma_g^+ - X^3\Sigma_g^-$) | 7600 | ~300 |
| | 8640 | ~20 |
| O $_2$ ($a^1\Delta_g - X^3\Sigma_g^-$) | 1.27 | ~30,000 |
| OH (M) | 2.8-4.0 | ~5,000 |

Table 2. Band systems and wavelengths of transitions of O_2 [Kuznetsovsky and Yarin, 1962].

| Transition | Band Systems | Band Wavelengths, Å | | | | Einstein Coefficient A, sec^{-1} |
|---------------------------------|-----------------------------|---------------------|-------|-------|-------|--|
| | | 0,0 | 0,1 | 1,0 | 1,1 | |
| $a^1\Delta_g - X^3\Sigma_g^-$ | Infrared atmospheric system | 12690 | 15800 | 10680 | 12800 | 1.9×10^{-4} |
| $b^1\Sigma_g^+ - X^3\Sigma_g^-$ | Atmospheric system | 7619 | 8645 | 6882 | 7708 | 0.14 |
| $b^1\Sigma_g^+ - a^1\Delta_g$ | Second infrared system | 19080 | 26630 | 15030 | 19380 | 2.5×10^{-3} |
| $A^3\Sigma_u^- - b^1\Sigma_g^-$ | First Herzberg system | 2856 | 2988 | 2794 | 2921 | $\sim 10^{-2}$ |
| $A^3\Sigma_u^- - b^1\Sigma_g^+$ | Broida-Gaydon system | 4567 | 4880 | 4412 | 4703 | |
| $B^3\Delta_u - X^3\Sigma_g^-$ | Third Herzberg system | | | | | $< 10^{-5}$ |
| $B^3\Delta_u - a^1\Delta_g$ | Chamberlain system | | | | | |
| $C^1\Sigma_u^- - X^3\Sigma_g^-$ | Second Herzberg system | 2761 | 2885 | 2714 | 2834 | $\sim 10^{-4}$ |
| $C^3\Sigma_u^- - X^3\Sigma_g^-$ | Schumann-Runge system | 2026 | 2092 | 1998 | 2062 | |

Table 3. The band systems of O_2 in the airglow spectrum [Evans and Llewellyn, 1970].

| Band System | Transition | Wavelength (Å or μm) | Day Airglow Radiance (kR) | Night Airglow Radiance (kR) |
|-----------------------------------|---------------------------------|-------------------------------|---------------------------------|-----------------------------------|
| Herzberg bands | $A^3\Sigma_u^+ - X^3\Sigma_g^-$ | 3100 - 5000 | No observation | 0.5 |
| Atmospheric System | $b^1\Sigma_g^+ - X^3\Sigma_g^-$ | 7619 (0,0) | 300 | ~8 |
| | | 8645 (0,1) | 15 | 0.4 |
| Infrared Atmospheric System | $a^1\Delta_g - X^3\Sigma_g^-$ | 1.27 (0,0) | | |
| | | 1.58 (0,1) | 25000 | 90 |

Table 4. O_2 atmospheric band radiances (kR) under auroral conditions, $I(5577) = 100$ kR [Vallance Jones and Gattinger, 1974].

| v'/v'' | 0 | 1 | 2 | 3 | 4 | 5 |
|----------|-----------------|----------------|----------------|----------------|---------------|---------------|
| 0 | 7619 (1200)+ | 8645 (58)* | | | | |
| 1 | 6882 | 7708 (13)* | 8742 (1.6) | | | |
| 2 | 6286 | 6968 (1.9)* | 7802 (6.8)* | 8844 (1.4) | | |
| 3 | | 6370 (0.40) | 7059 (6.2)* | 7901 (12) | 8950 (3.9) | |
| 4 | | | 6457 (0.30) | 7154 (2.8)* | 8006 (3.1) | |
| 5 | | | | 6457 (0.55) | 7255 (3.5) | 8118 (2.3) |

The wavelength for each band is given in angstroms. The value in parentheses are corresponding radiance values.

*Uncertainty less than 25%.

+Derived from $I(0,1)$ from transition probability.

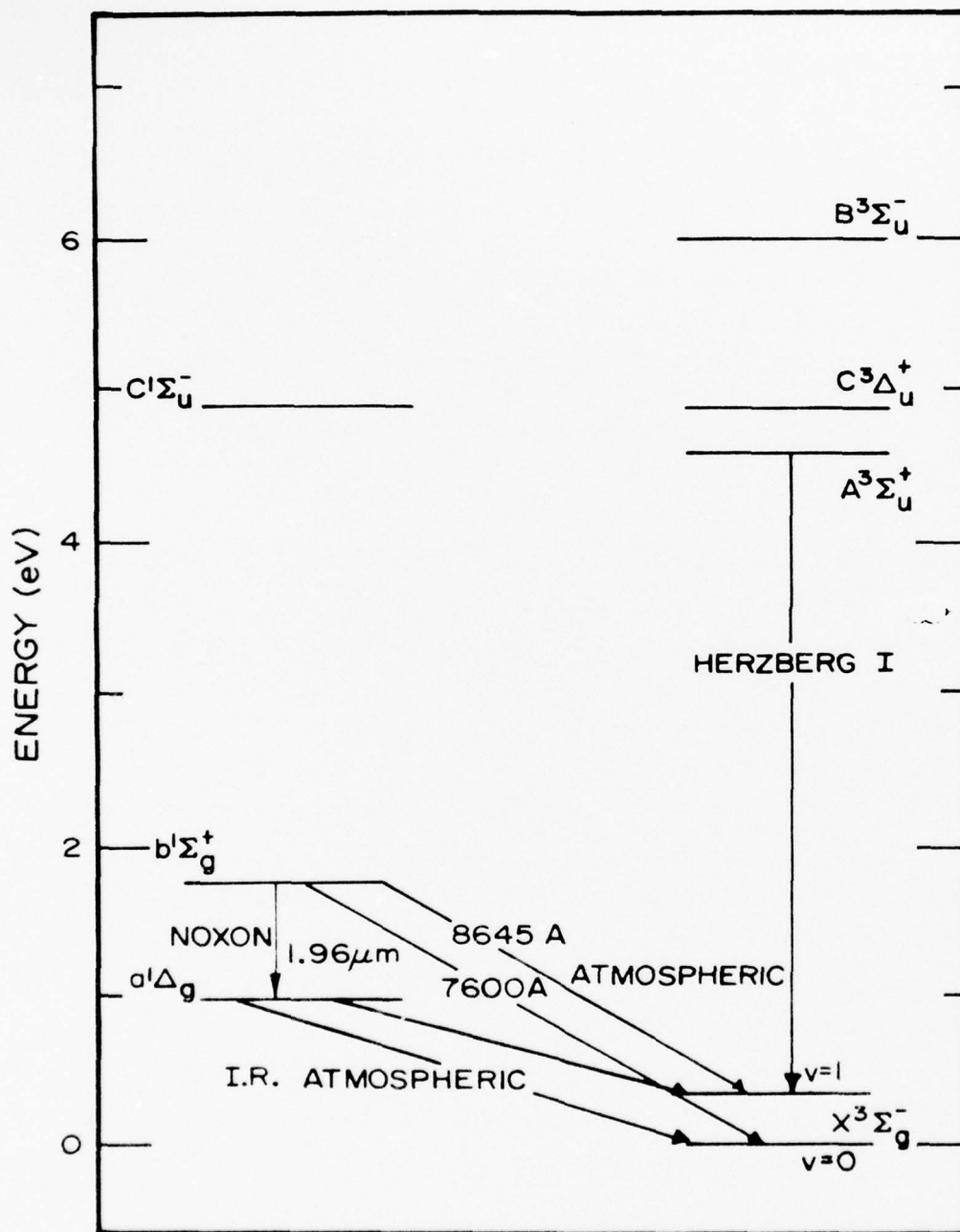


Figure 1. Simplified energy levels and transitions of O_2 .

By using the Boltzmann probability distribution formula, the ratio of abundance of $O_2^*(X^3\Sigma_g^-, v=1)$ to $O_2(X^3\Sigma_g^-, v=0)$ can be well approximated by the expression:

$$r(T) = \frac{O_2^*}{O_2} = \exp \left[- \frac{hc\nu_1}{kT} \right] \quad (1)$$

where

h = Planck's constant, 6.625×10^{-27} erg·sec

c = Velocity of light in vacuum, 2.99793×10^{10} cm/sec

ν_1 = Wavenumber of the transition from the first vibrational state ($X^3\Sigma_g^-, v=1$) to the ground state ($X^3\Sigma_g^-, v=0$), 1556 cm^{-1}

k = Boltzmann's constant, 1.38044×10^{-16} erg/deg

T = Temperature, in °K

Values of $r(T)$ for various temperatures are listed in a table in Appendix B. In the tropospheric condition, $r(T)$ is always less than about 2×10^{-4} .

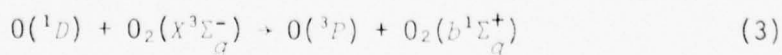
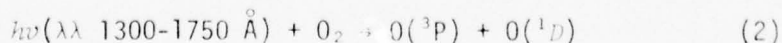
Although some measurements have been taken by rocket observations [Wallace and Huntten, 1968], there is considerable advantage in being able to economically measure the emissions of O_2 in the mesosphere from ground-based observatories over a long period of observation.

This study was done on the (0,1) band of the atmospheric system of O_2 . The data analyzed here were taken by USU personnel in March, 1975 using the USU *Argus* Mobile Aeronomy Observatory which at the time was located at Poker Flat, Alaska.

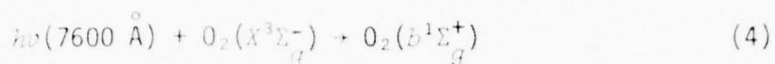
Emission Mechanisms

In their paper dealing with rocket observations of the atmospheric bands in the day airglow, Wallace and Huntten [1968] suggest three sources of $O_2(b^1\Sigma_g^+)$ which would be expected to occur only in a sunlit atmosphere. They are:

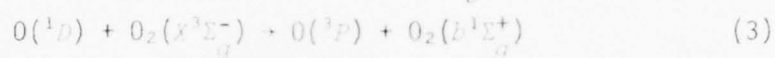
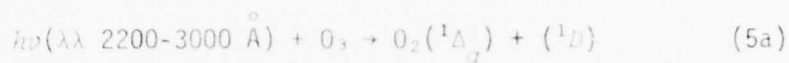
1. Energy transfer from $O(^1D)$, dominant above 100 km



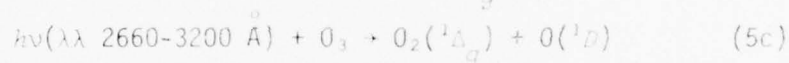
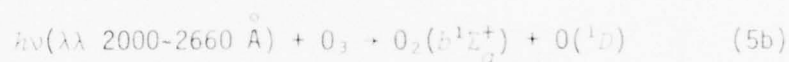
2. Resonance scattering, dominant in the region from 65 km to 100 km



3. Photolysis of ozone, dominant in the region from 35 km to 65 km and probably important up to 100 km



Later work has shown that the number density of excited oxygen molecules is closely related to the number density of ozone. Reaction (4) can be replaced by [Shimanaki and Laird, 1972]



which seems to dominate production in daylight from 40 to 100 km altitude. Figure 2 shows altitude profiles for O_3 , O_2 and the temperature for arctic winter conditions.

Both morning and evening conditions can be considered as a transition period between the day airglow, in which resonance radiations are dominant, and the night airglow, in which chemiluminescence becomes important. The morning twilight enhancement greatly exceeds that in the evening in the 80 to 100-km region [Norson, 1975]; the reason for this is the production of $\text{O}_2(^1\Sigma_g^+)$ by energy transfer from $\text{O}(^1D)$ produced in ozone photolysis at the same altitude. At sunset, the production of $\text{O}(^1D)$ in O_3 photolysis occurs only above 160 km [Norson and Johanson, 1972], and the resulting yield of $\text{O}_2(^1\Sigma_g^+)$ is negligible.

In the night airglow, the absence of sunlight renders chemical and ion-electron recombination reactions the dominant sources of $\text{O}_2(^1\Sigma_g^+)$. The resonance scattering that predominates during daytime and twilight conditions is relegated to a minor role. The excited states of molecular oxygen can be formed by three-body recombination:

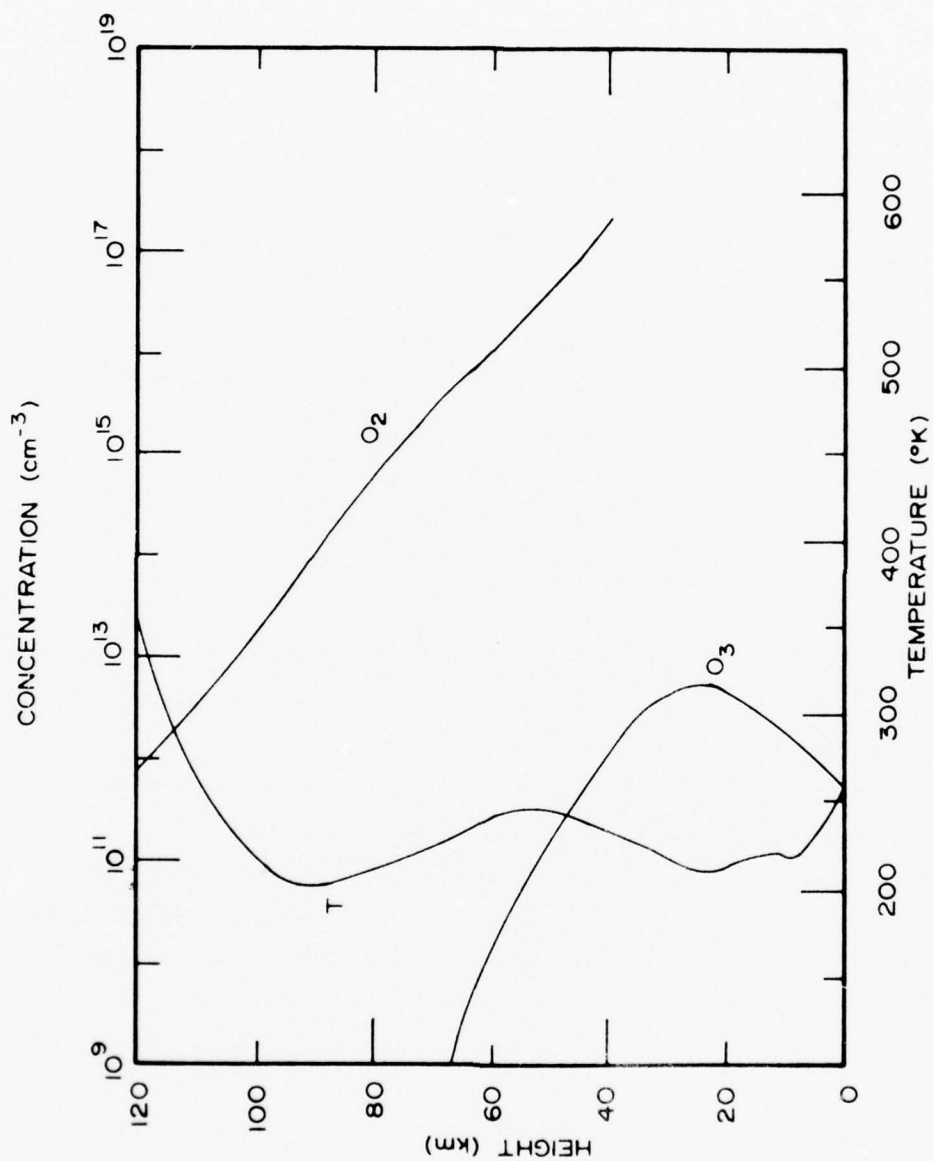
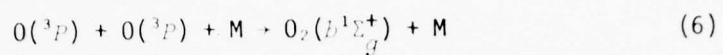
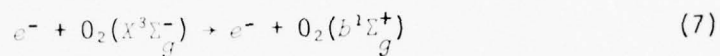


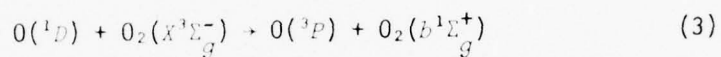
Figure 2. Typical average altitude profiles for $[O_2]$, $[O_3]$ and temperature for winter conditions at 60° latitude [Shimazaki and Laine, 1972].



Under auroral conditions the metastable states of molecular oxygen, $O_2(b^1\Sigma_g^+)$ in particular, can be produced by secondary auroral electrons, that is:



The $O_2(b^1\Sigma_g^+)$ can also be formed under auroral conditions by thermal collisions with metastable oxygen atoms:



OBJECTIVES

The objective of this study is to estimate the rotational temperatures of $O_2(b^1\Sigma_g^+ \rightarrow X^3\Sigma_g^-)$ atmospheric (0,1) band at 8645 Å in the airglow by the following steps:

1. Obtain the observed spectra of the night airglow.
2. Compute the synthetic spectra at different temperatures for an appropriate theoretical model.
3. Optimize a technique for comparing observed spectra with synthetic spectra of different rotational temperatures.
4. By the comparison of the observed spectra with synthetic spectra ascertain the apparent rotational temperatures of $O_2(b^1\Sigma_g^+)$ radiation of the night airglow.

SYNTHETIC SPECTRA

Line Spectrum

The radiance of an emission line in the infrared rotational spectrum or rotation-vibrational spectrum not only depends on the Boltzmann distribution function but also depends on the quantum number of the upper states. The emission radiance for a given line can be expressed as: [Herzberg, 1950]

$$I_{em} = \frac{2C_{em}\nu^3}{Q_P} \times S_{J'} \times \exp\left[\frac{-B_{v,J'}(J'+1)hc}{kT}\right] \quad (8)$$

where

I_{em} = The radiance of an emission line, in photon $\text{sec}^{-1}\text{cm}^{-2}\text{sr}^{-1}$

C_{em} = The emission constant

ν = The wavenumber of each transition which has been calculated and listed in Table C.2

Q_P = The partition function

$$= \sum_{\substack{J=0 \\ \Delta J=2}}^{20} (2J+1) \times \exp[-F'(J) \times hc/kT]$$

J' = The total quantum number of the upper state

$S_{J'}$ = The line strength of each transition.

The ratio of splitting constant λ to the molecular rotational constant B_v , namely, $\lambda/B_v = \frac{1.934}{1.391328} \sim \frac{3}{4}$ (see Appendix C), $S_{J'}$ can be expressed as follows [Schlapp, 1936]:

$$\begin{aligned} S_{J'} &= \frac{1}{2}(J'+2) && \text{for } P_P \text{ branch} \\ S_{J'} &= \frac{1}{2}(J'+\frac{3}{4}) && \text{for } P_Q \text{ branch} \\ S_{J'} &= \frac{1}{2}(J'+\frac{1}{4}) && \text{for } R_Q \text{ branch} \\ S_{J'} &= \frac{1}{2}(J'-1) && \text{for } R_R \text{ branch} \end{aligned} \quad (9)$$

This relationship is based upon an assumption of rotational equilibrium in the upper state. One should justify this for the system of interest.

In this paper, only the relative radiance is needed. The attempt is by comparison of the shapes of theoretical band profiles with measured profiles to deduce the apparent rotational temperature. The emission constant C_{em} in Equation (8) need not be evaluated in the calculation of relative radiance. The relative radiances of line spectrum at a temperature of $T=210^\circ\text{K}$ are shown in Figure 3. This band shows two wings, the P wing which includes P_P branch and P_Q branches and an R wing which includes an R_R branch and a R_Q branch. The band center is at 11564 cm^{-1} . The computer programs, named O2EMI and SORT, which generate the wavenumber and radiance of each line and sorted in the order of increasing wavenumber respectively, are listed in Appendix D.

Synthetic Spectrum

For each particular wavenumber point of the band, the radiance can be computed by the formula as:

$$I_L = \sum_{j=1}^N I_j \times \frac{\sin X_{L,j}}{X_{L,j}} \times \left[1 - \left(\frac{\Delta v_{L,j}}{4\Delta v} \right)^2 \right]^2 \quad (10)$$

where

$$\Delta v_{L,j} = |v_L - v_j|, \text{ in } \text{cm}^{-1}, |\Delta v_{L,j}| \leq 4 \times \text{RES}$$

$$v_L = \text{The wavenumber of any point } L \text{ in the band in } \text{cm}^{-1}$$

$$v_j = \text{The wavenumber of one line in line spectrum in } \text{cm}^{-1}$$

$$\Delta v = \text{The resolution, which means the wavenumber interval from the central maximum to first minimum of } \frac{\sin X}{X} \text{ function}$$

$$I_j = \text{The relative radiance of one line in the line spectrum}$$

$$X_{L,j} = \frac{\pi \times \Delta v_{L,j}}{\Delta v}$$

$$N = \text{Total number of emission lines, namely, 77 for } j=0 \text{ to } 22$$

$$\text{RES} = \text{Resolution}$$

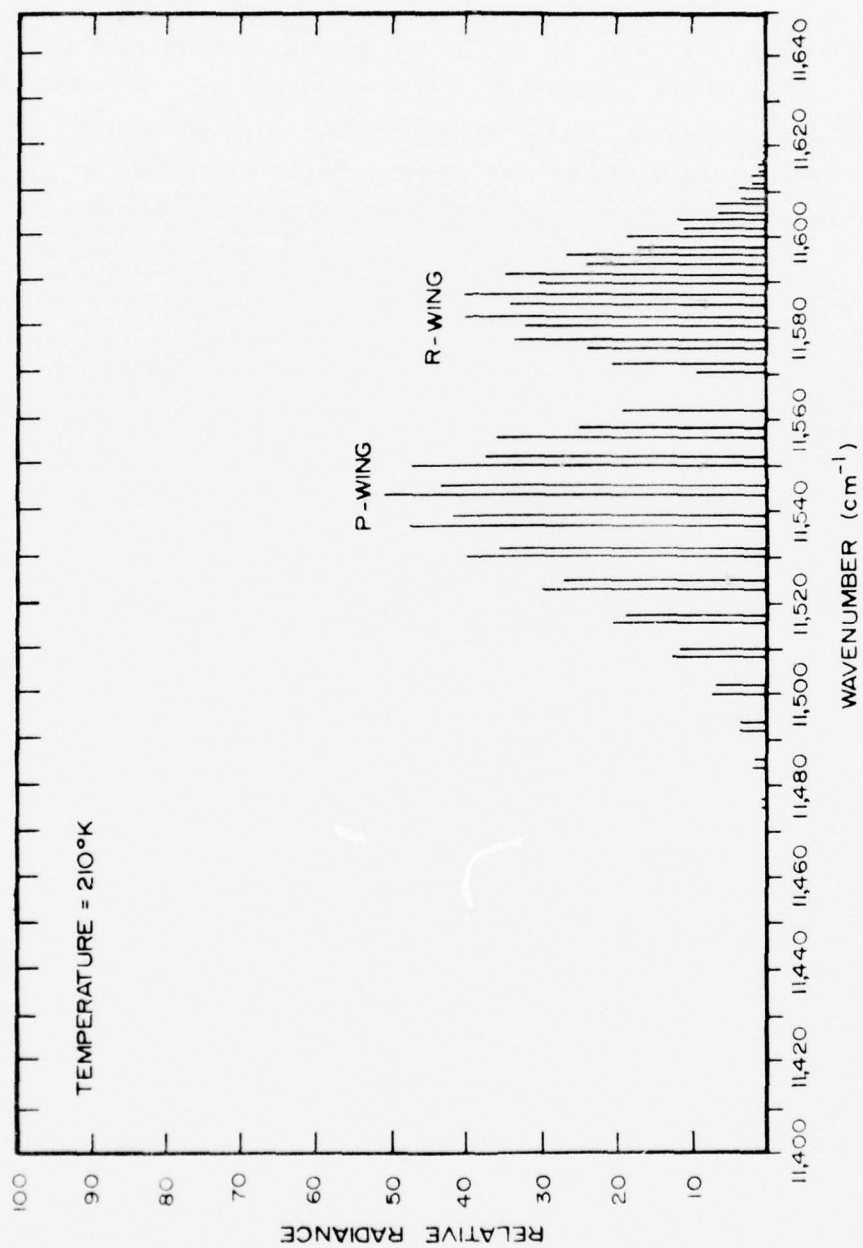


Figure 3. $O_2(\Delta^1\Sigma_g^+)$ atmospheric (0,1) band synthetic line spectrum at $T = 210^\circ K$.

$$\text{The apodizing function} = \left[1 - \left(\frac{\Delta\nu_{ij}}{4\Delta\nu} \right)^2 \right]^2$$

Taking into account the resolution function and the apodizing effect of the filter, it is assumed that the value of the spectral radiance can be neglected beyond the fourth minimum on each side of the $\frac{\sin x}{x}$ function contributed by the radiance of a single emission line. The spectral radiance at each wavenumber point of the band region is the sum of all the contributions at this point. The relative radiance of the whole band has been calculated with a 0.5 cm^{-1} interval over the band region for comparison with observed spectra.

The computer program, named CNVLS, is listed in Appendix D. The spectral radiance profiles for different temperatures and resolutions are shown in Figures 4, 5, and 6. In Figures 4 and 5, the envelope of the line spectrum becomes smoother as the resolution interval increases. Two spectra for $T=150^\circ\text{K}$ and $T=250^\circ\text{K}$, both at 3.0 cm^{-1} resolution, are shown in Figure 6. The peak of R wing and the peak of P wing each shift away from the band center when the temperature increases.

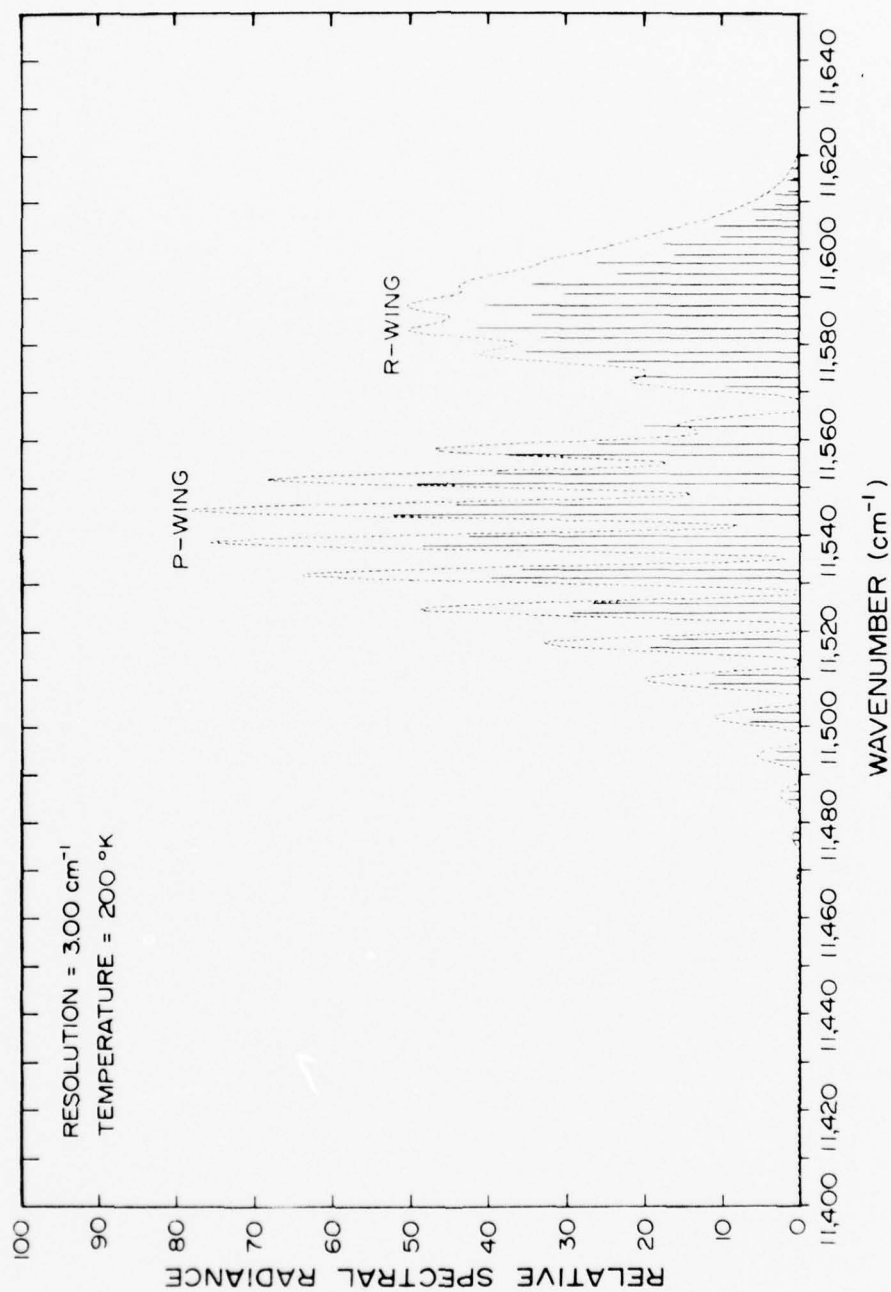


Figure 4. The synthetic spectrum of $0_2(0_2^+)(1_2^+)$ atmospheric ($0,1$) band with 3.0 cm^{-1} resolution.

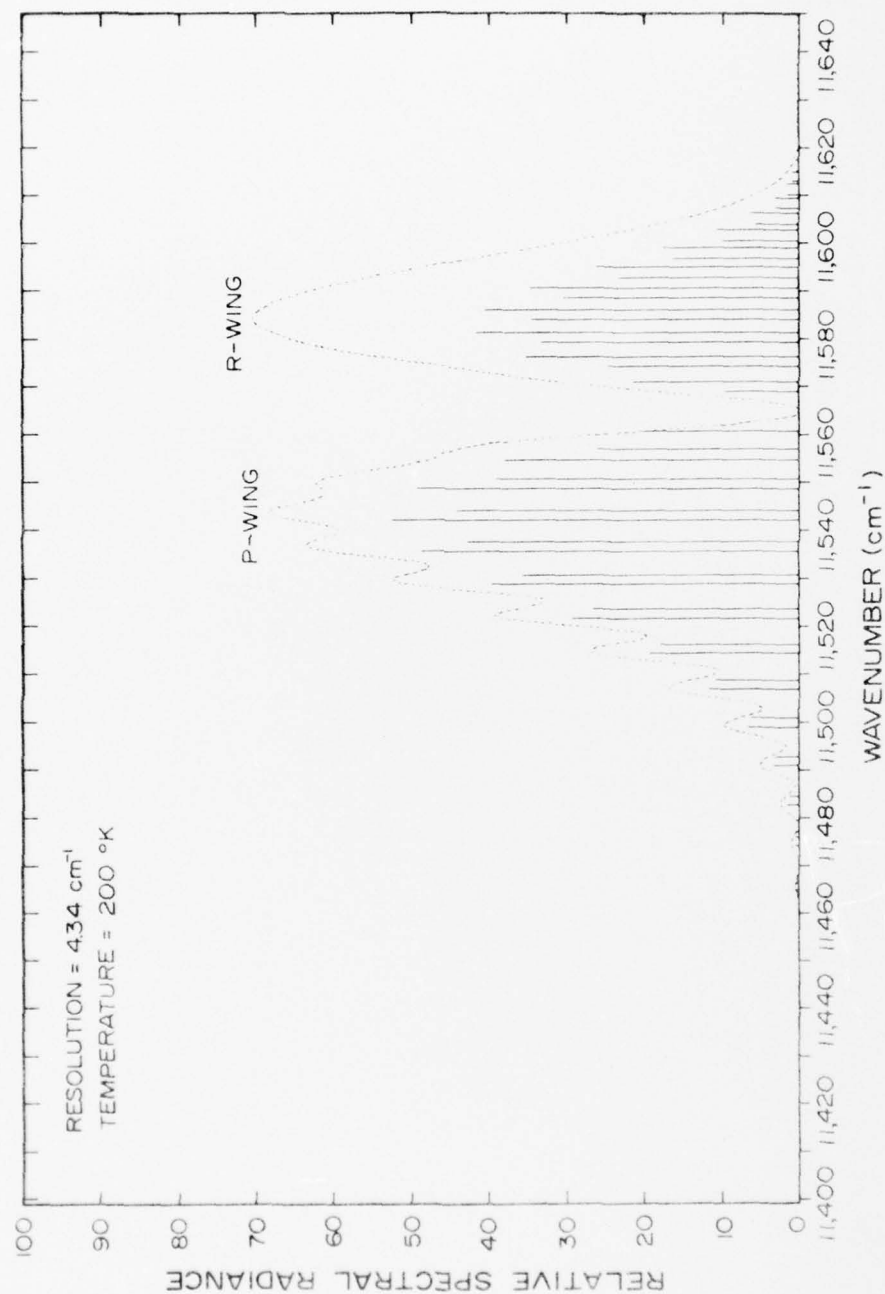


Figure 5. The synthetic spectrum of $\text{O}_2(b^1\Sigma_g^+)$ atmospheric (0,1) band with 4.34 cm^{-1} resolution.

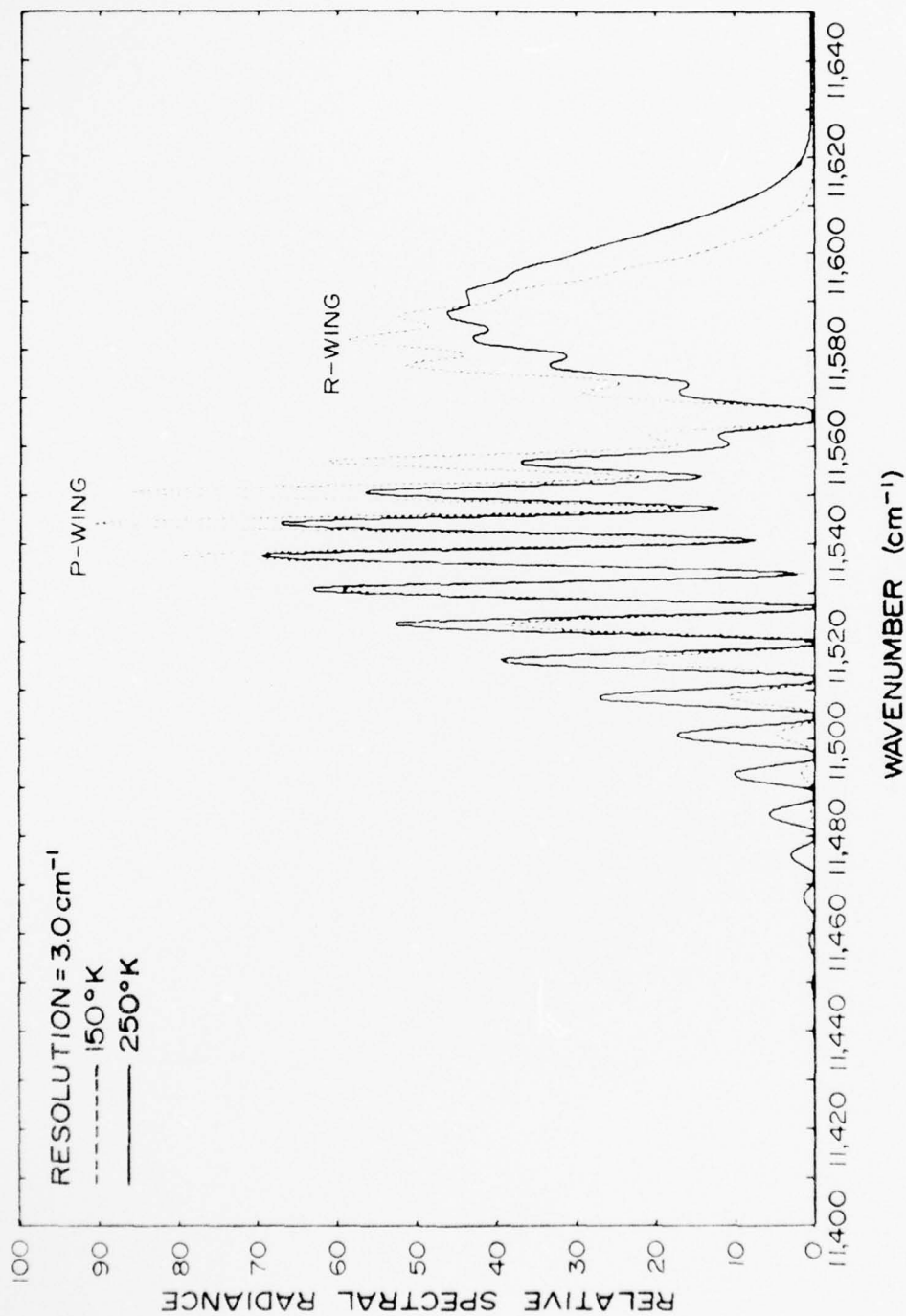


Figure 6. Theoretical spectra of $0_2(1_1^+)$ atmospheric (0,1) band at different temperatures.

INSTRUMENT DESCRIPTION

The measuring system for the airglow emission is a large-aperture field-widened interferometer-spectrometer system which has been designed and developed by the Electro-Dynamics Laboratories of the Utah State University [Despain *et al.*, 1970]. A simplified schematic diagram of this interferometer-spectrometer system is shown in Figure 7. Two wedge end mirrors are used instead of the simple mirrors of a conventional Michelson interferometer. One of the wedge end mirrors is fixed and the other is driven by a mirror carrier system which includes a laser beam interferometer to record the position of the movable wedge end mirror. The salient features of the system are: (1) field of view widened to 5° full angle; (2) a 5-cm clear aperture; and (3) a 5-cm drive capability.

Suppose that a beam of light is divided by the beam splitter into two mutually coherent beams, as in the Michelson interferometer, and these beams are reunited after traversing different optical paths. The reunited beam goes through a lens and is detected by a photodetector. If the light is not monochromatic but has a spectral composition given by the power spectrum $G(\nu)$, where ν is the wavenumber, then the intensity of the reunited beam varies in a manner that depends on the particular optical spectrum. By recording the intensity as a function of the path difference, or the position of the movable wedge end mirror, the power spectrum $G(\nu)$ can be deduced. We can write the intensity of the reunited beam $I(x)$ as:

$$I(x) = \frac{1}{2} I(0) + \frac{1}{2} \int_{-\infty}^{\infty} G(\nu) e^{i\nu x} d\nu \quad (11)$$

or

$$W(x) = 2I(x) - I(0) = \int_{-\infty}^{\infty} G(\nu) e^{i\nu x} d\nu \quad (12)$$

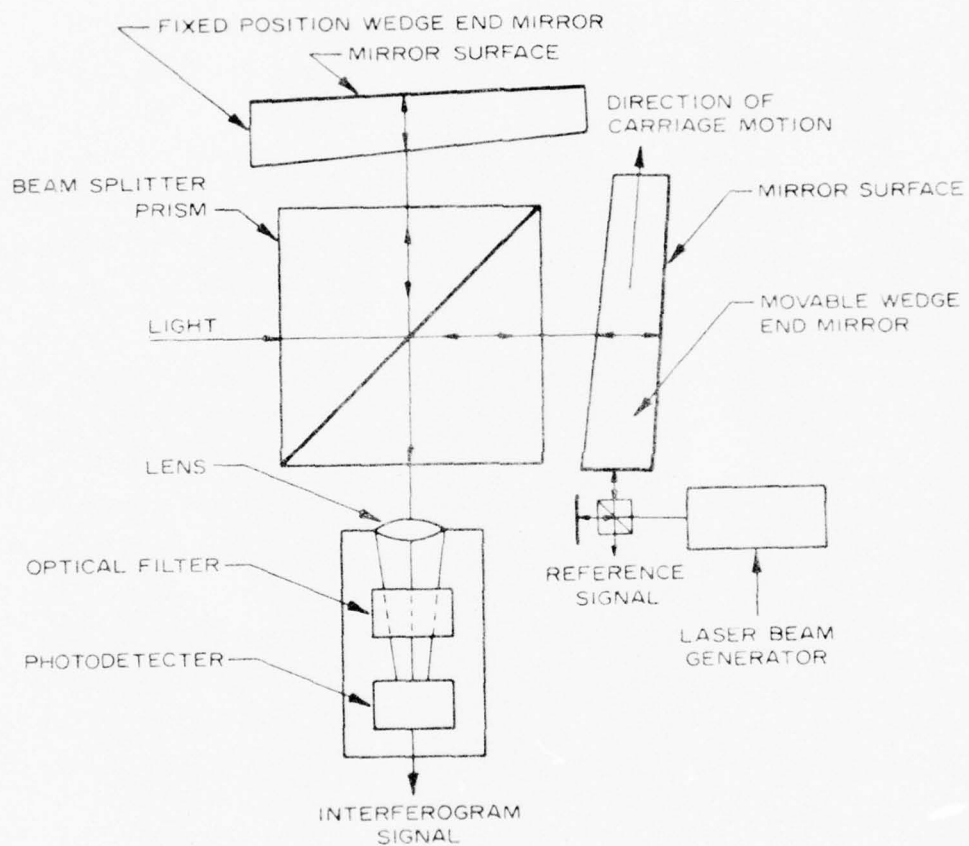


Figure 7. A simplified schematic diagram of the EDL interferometer-spectrometer system.

where $I(0)$ is the intensity for zero path difference and x is the path difference. Therefore, $W(x)$ and $G(v)$ constitute a Fourier transform pair. Accordingly, we can write;

$$G(v) = \frac{1}{2\pi} \int_{-\infty}^{\infty} W(x) e^{-i v x} dx \quad (13)$$

From the output of the detector, $W(x)$ is the output voltage signal which depends on the position of the movable wedge end mirror recorded by the laser as a reference signal. Then, the Equation (13) can be solved by the Fourier transform computer program.

The resolution capability of a Michelson interferometer is generally taken to be;

$$\Delta v = \frac{1}{\delta} \quad (14)$$

where $\Delta v = v_2 - v_1$, is the difference in wavenumber between two resolvable adjacent monochromatic lines and δ is the maximum optical path difference. The relationship between the optical path difference and distance of motion of the wedge prism along its apparent mirror image plane in the field-widened system can be expressed as [Baker, 1976]:

$$\delta = 2x \left[n \sin \alpha + \tan \gamma \left(\frac{n^2 \sin^2 \alpha - 1}{\cos \beta} \right) \right] \cos \gamma \quad (15)$$

where x is the drive length, n is the index of refraction, α is the prism angle, $\beta = \sin^{-1}(n \sin \alpha)$, and $\gamma = \tan^{-1}(\tan^2 \alpha / \tan \beta)$. For the values $\alpha = 8^\circ$ and $n = 1.5$;

$$\delta = 0.21x \quad (16)$$

The drive length x can be derived as;

$$x = N_e \times \frac{\lambda}{2} \times N_s \quad (17)$$

where N_c is the number of cycles of the reference signal between each sample, λ_L is the wavelength of laser and N_s is the total number of sample points in an interferogram. For the values $N_c = 4$, $\lambda_L = 6328 \text{ \AA}$ and $N_s = 16384$, the drive length x is equal to 2.0735 cm or $\delta = 2.296 \text{ cm}^{-1}$.

SPECTRAL COMPARISON METHOD

Comparison Technique

While recording the interferograms, the incoming sky radiation was limited on the long wavelength side by the response of the photo-detector, and on the short wavelength side by a filter. Figure 8 shows a typical spectrum obtained by digitizing the interferogram, computing the spectrum by using the fast Fourier transform (FFT) and plotting the amplitude.

Before using such a spectrum, it must be corrected for the instrument response. This was accomplished by obtaining the spectrum of a radiation source of known characteristics, and ascertaining a correction factor as a function of wavelength.

An interferogram was recorded with the instrument pointing at the full moon, and the corresponding spectrum was computed and plotted. The source spectrum was treated as a blackbody at a temperature of 6000°K, which the solar spectrum closely approximates in this wavelength region. From Planck's blackbody distribution equation:

$$\rho_T(\lambda) = \frac{8\pi hc}{\lambda^5} \times \frac{1}{\exp[hc/k\lambda T] - 1} \quad (18)$$

where

ρ_T = Energy density per unit volume per unit wavelength, in erg/cm⁴.

The relative intensities for different wavelengths of solar radiation can be derived by:

$$\frac{\rho_T(\lambda_1)}{\rho_T(\lambda_2)} = \frac{\lambda_2^5 \times [\exp(hc/k\lambda_2 T) - 1]}{\lambda_1^5 \times [\exp(hc/k\lambda_1 T) - 1]} \quad (19)$$

Figure 9 shows a smooth plot of a portion (11457 to 11614 cm⁻¹) the spectrum obtained from observing the full moon with the same

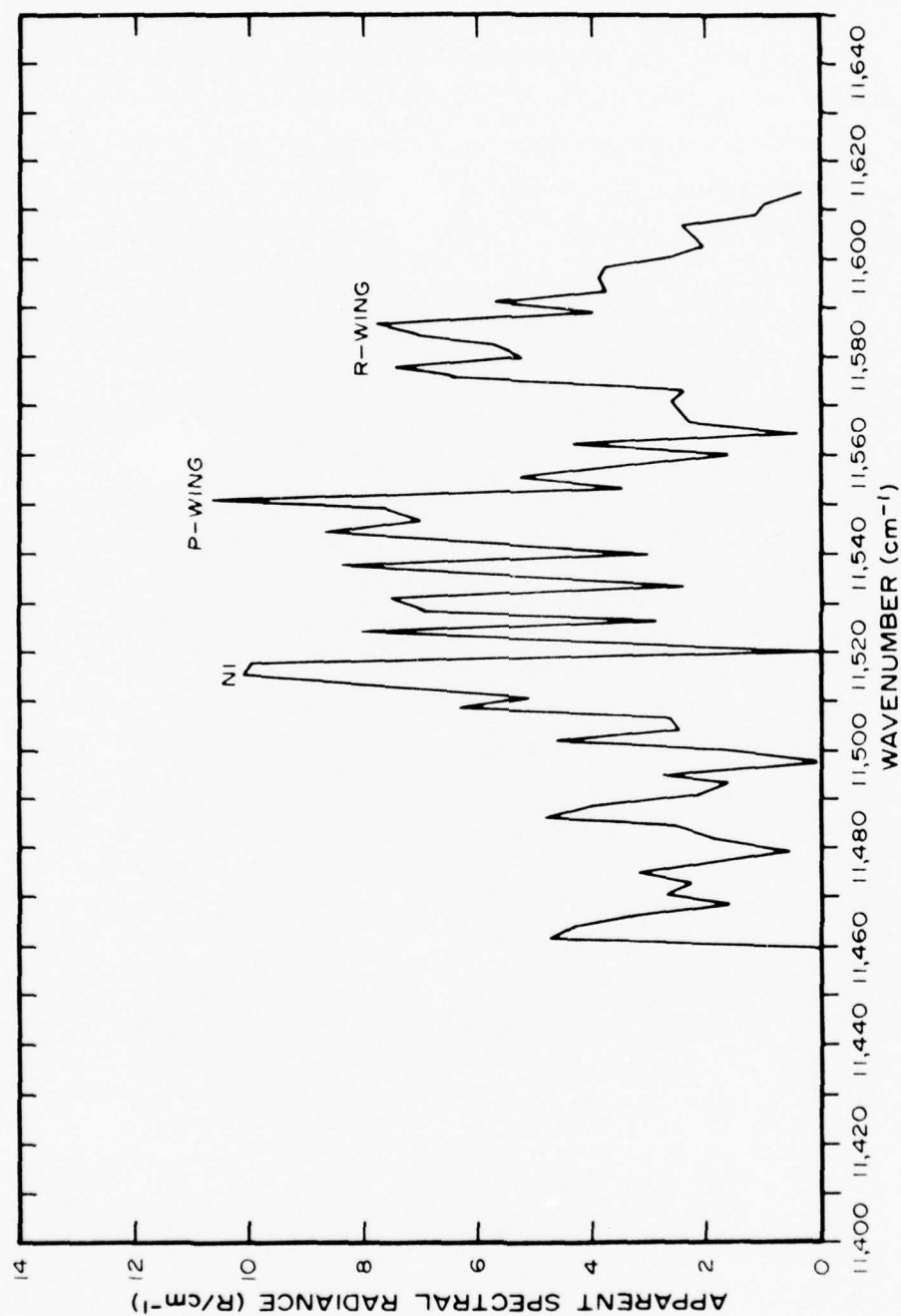


Figure 8. The night airglow spectrum of $O_2(b^1_2g)$ atmospheric (0,1) band measured at Poker Flat, Alaska at 8:45 hrs. UT ($\lambda = 121.03$) on March 1, 1975.

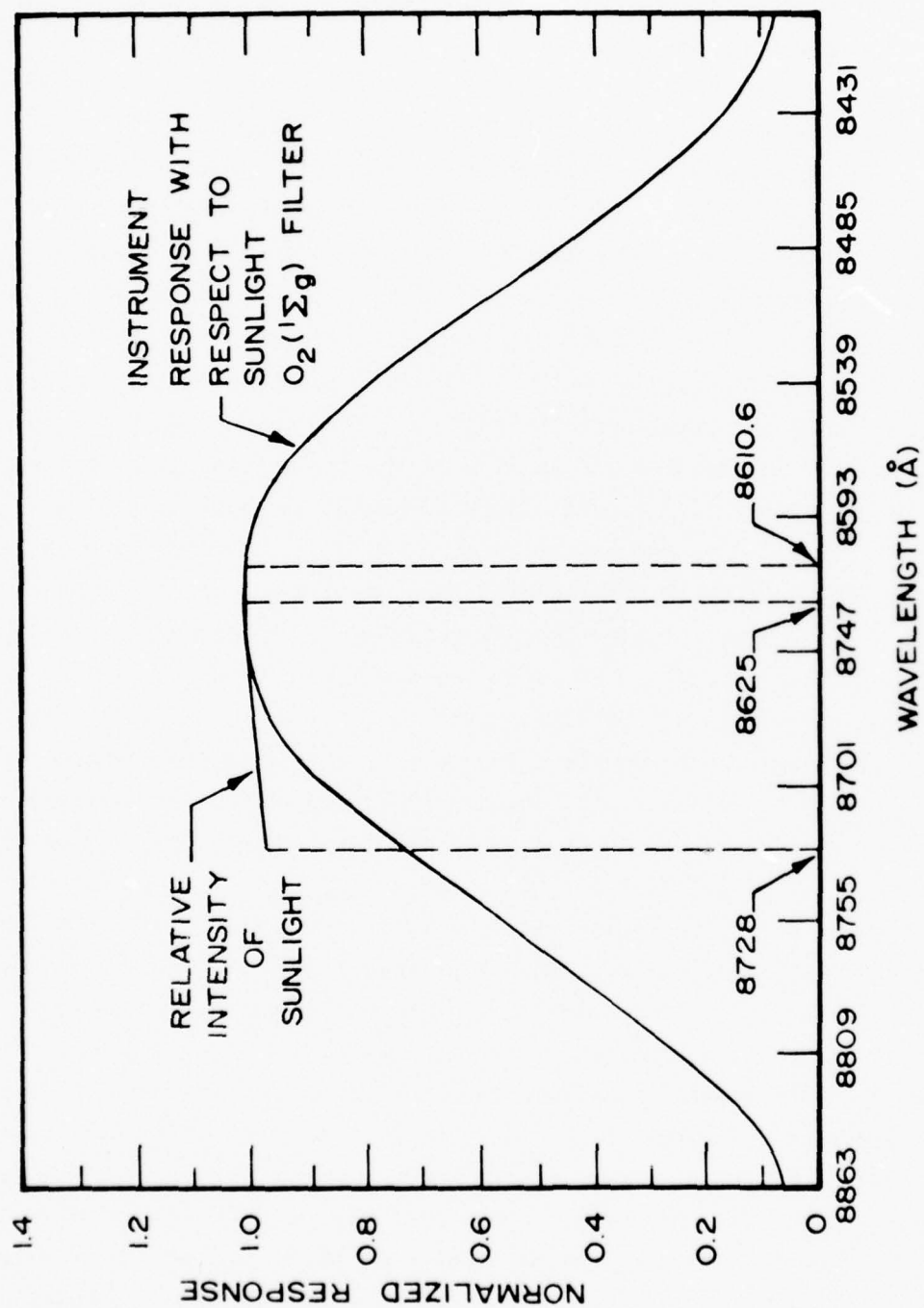


Figure 9. The relative intensity of sunlight and the instrument response with respect to sunlight.

spectrometer. Also shows a plot of the relative spectral radiance of sunlight modeled as a 6000°K blackbody source. The instrument correction for any wavenumber in this region is the ratio of the relative spectral radiance of the source to the relative intensity of the observed spectrum, which is shown in Figure 10. The values of instrument response corresponding to each sample point over the band are listed in Appendix E.

The spectral radiance at each sample point of the $O_2(b^1\Sigma_g^+)$ spectrum is instrument corrected by dividing the instrument response (Fig. 10) and then is normalized by dividing by the total radiance of the band. For the spectrum given in Figure 8 for 8:45 hrs. UT (solar zenith angle $\alpha = 211^\circ$) taken at Poker Flat, Alaska, on March 1, 1975, the apparent zenith radiance of the $O_2(b^1\Sigma_g^+)$ (0,1) airglow band was 500 rayleighs. This value is uncorrected for atmospheric extinction. Then each corrected sample value is treated as radiance of one line in the theoretical line spectrum, and interpolated by $\frac{\sin X}{X}$ function with a resolution equal to 3.0 cm^{-1} .

A family of theoretical spectra has been generated over the range from 140 to 300°K in 10°K steps. These were convolved to a resolution of 3.0 cm^{-1} . Values of the spectral radiance of both observed and theoretical spectra were calculated at sample points spaced each 0.5 cm^{-1} over the range from 11400 cm^{-1} to 11650 cm^{-1} .

The range of wavenumbers for optimal band-shape comparison were limited to 11535.9 to 11616.3 cm^{-1} because of overlap with other spectral features of the airglow and aurora [Wallace and Chamberlain, 1959]. These include multiplet 1 of NI(11431.2 - 11517.3 cm^{-1}), the (2,1) band of the First Positive system of N_2 in the region 11461.8 - 11530.6 , and the $P_1(7)$ and $P_2(7)$ lines of the (6-2) band of OH(11628.5 and 11640.7 cm^{-1}).

The best-fit band shape comparison for rotational temperature estimating proceeds as follows. The total band radiances of both the synthetic and the experimental spectra within the selected comparison range are forced to equality by change of scale factor. The difference between the radiances of the observed and the theoretical spectra were calculated at each 0.5 cm^{-1} in the range. The sum of the absolute values of the differences, $\sum |di|$, the sum of squares of the values of the differences, $\sum (di)^2$, and the sum of relative absolute values of the difference, $\sum \frac{|di|}{Ri}$, were all calculated for the specified rotational temperatures. These vlaues

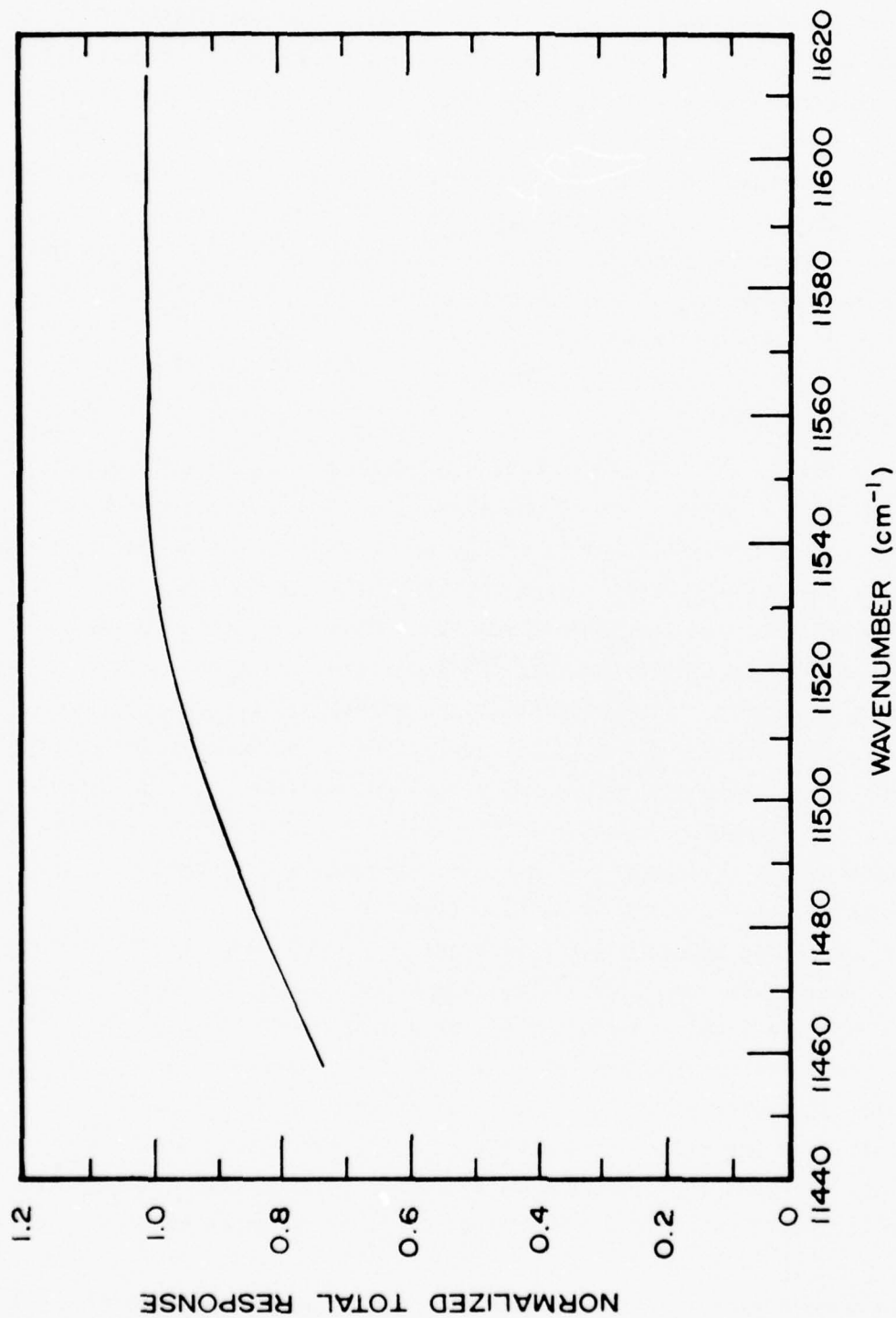


Figure 10. The normalized total response with respect to wavenumber over the range of $O_2(b^1\Sigma_g^+)$ atmospheric (0,1) band.

change from one rotational temperature to another, and the minimum of difference was found by a curve fitting technique as shown in Figure 11.

The observed spectrum processing program, DTPRS, the comparison program and the numerical results associated with Figure 11 are listed in Appendix D. As expected, the variance of temperature given by the different comparison techniques was dependent upon the signal to noise ratio. The sum of the squares technique was adopted as optimal because it empirically gives the best weighting of the various portions of the spectrum according to strength of signal relative to noise.

Discussion of Results

All of the $O_2(b^1\Sigma_g^+)$ spectra considered here were taken at Poker Flat, Alaska, on March 1, 1975. Rotational temperature for each spectral scan calculated by the curve-fitting technique are listed in Table 5 using three different approaches as discussed in the previous section. The $\Sigma(di)^2$ approach emphasizes the portions of the band which have higher value of spectral radiance in comparison with the lower ones which are more affected by the noise. Figure 12 shows the rotational temperatures computed using both the $\Sigma|di|$ and $\Sigma(di)^2$ approaches. The results are generally in good agreement with each other and also in comparison with the result from using the weighting function $\Sigma \frac{|di|}{R_i}$, where R_i is the radiance of observed spectrum at the comparison point. The agreement is best when the $O_2(b^1\Sigma_g^+)$ is brightest, as is to be expected.

The comparison approach was also tried on two coadded (signal averaged) spectra. The results of $\Sigma(di)^2$ again show a much better agreement between the apparent rotational temperature of the coadded spectrum and the average rotational temperature over the same time interval. In Figure 12, the result calculated using $\Sigma \frac{|di|}{R_i}$ curve shows more temporal fluctuation than result from the other summing methods. The average apparent rotational temperature over the time interval using $\Sigma(di)^2$ is about 211°K*; this is close to the expected ambient temperature at about 90 km as shown in Figure 2.

*Points were ignored if the difference between computed temperatures using $\Sigma|di|$ and $\Sigma(di)^2$ was $>10^\circ\text{K}$.

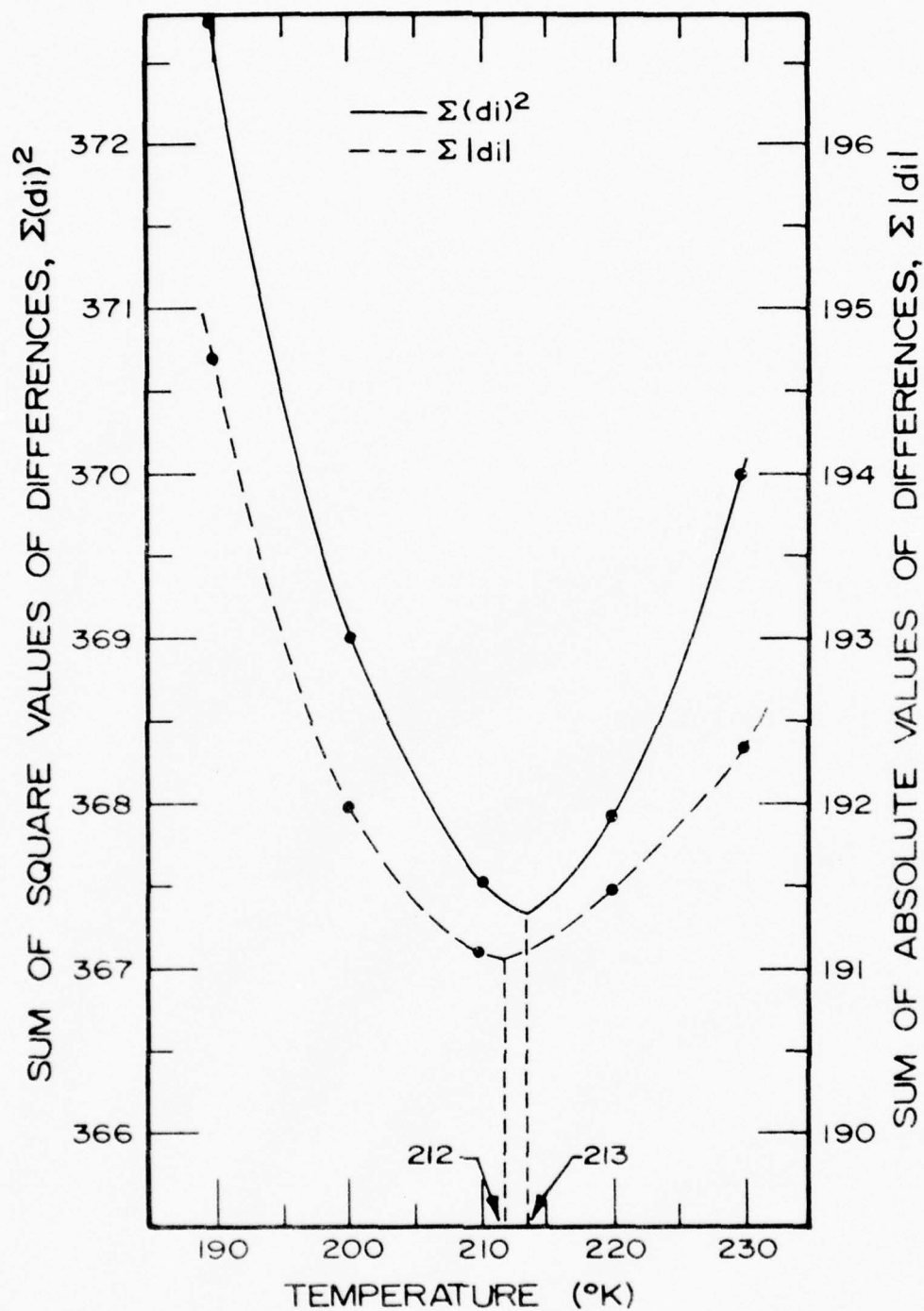


Figure 11. Comparison of theoretical models of different temperatures and measured spectrum taken at Poker Flat, Alaska, on March 1, 1975 at 8:43-8:46 hrs. UT.

Table 5. Rotational temperatures ($^{\circ}\text{K}$) of $\text{O}_2(b^1\Sigma_g^+)$ (0,1) band calculated using three approaches.

| Time (hrs. UT) | Sum of Relative Absolute Differences $\Sigma(di /Ri)$ | Sum of Absolute Differences $\Sigma di $ | Sum Differences of Square $\Sigma(di)^2$ |
|-------------------|--|--|--|
| 8:30-8:58* | 220 | 203 | 221 |
| 8:58-9:59* | 224 | 201 | 216 |
| 8:31-8:34 | 290 | 260 | 244 |
| 8:34-8:38 | 194 | 193 | 190 |
| 8:46-8:50 | 264 | 230 | 240 |
| 8:50-8:54 | 200 | 192 | 188 |
| 8:54-8:58 | 260 | 241 | 230 |
| 9:02-9:06 | 222 | 230 | 240 |
| 9:14-9:18 | 213 | 252 | 267 |
| 9:18-9:22 | 206 | 199 | 215 |
| 9:27-9:31 | 180 | 182 | 202 |
| 9:31-9:35 | 182 | 180 | 189 |
| 9:35-9:39 | 253 | 251 | 241 |
| 9:39-9:43 | 220 | 212 | 213 |
| 9:43-9:47 | 240 | 235 | 248 |
| 9:47-9:51 | 182 | 181 | 171 |
| 9:51-9:55 | 235 | 235 | 245 |
| 9:55-9:59 | 189 | 189 | 195 |
| 8:30-8:58** | 242 | 223 | 218 |
| 9:02-9:59 | 211 | 213 | 221 |
| Over all Avg. | 226 | 219 | 220 |

*Coadd spectrum.

**Average temperature over the time period.

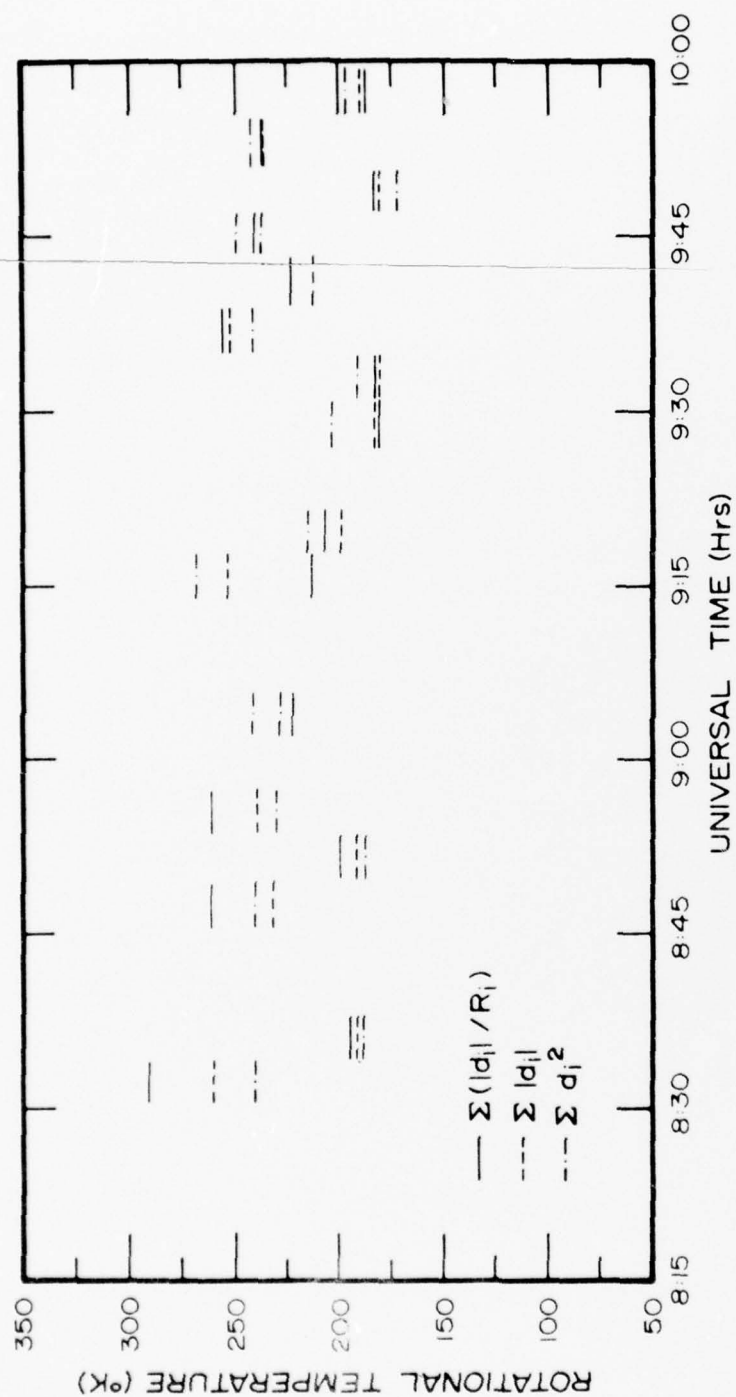


Figure 12. Apparent rotational temperature of $O_2(b^1\Sigma_g^+)$ atmospheric (0,1) band of each scan on March 1, 1975.

Of concern is whether $O_2(b^1\Sigma_g^+)$ state rotational temperature equilibrium has been achieved prior to radiative relaxation by sufficient collisions with the ambient atmospheric molecules (primarily N_2). The collision frequency per molecule f can be written as;

$$f = n\bar{c}\sigma \quad (20)$$

where

n = the density of air, cm^{-3}

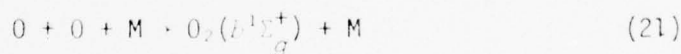
$\bar{c} = \sqrt{\frac{8kT}{\pi m}}$, the average speed, k is Boltzmann's constant, T is the absolute temperature, m is mass of molecule

$\sigma = 2\pi r^2$, the projected area of a spherical molecule;

r = the internuclear distance, 1.904×10^{-8} cm for N_2 ,
 1.207398×10^{-8} cm for O_2 [Herzberg, 1950]

At 90 km, $n \approx 10^{14} \text{ cm}^{-3}$, $T \approx 200^\circ\text{K}$, $m = 4.7816 \times 10^{-23}$ g/molecule, and $\bar{c} = 3.834 \times 10^4$ cm/sec. Therefore, 3.5×10^3 /sec. The life-time of $O_2(b^1\Sigma_g^+)$ is approximately to 12 sec [Norxon, 1970]; so thermal rotational equilibrium may be achieved.

Theoretical vertical profiles of the volume emission rate for the $O_2(b^1\Sigma_g^+)$ (0,1) band of the night airglow are given in Figure 13 [Barth, 1961; Colegrove *et al.*, 1966]. The peaks of both curves occur around 90 km. The oxygen excitation in the 90 km region is attributed to the Chapman reaction:



By comparison, a rocketborne measurement of the daytime airglow volume emission rate profile of $O_2(b^1\Sigma_g^+)$ atmospheric (0,1) band as given by Wallace and Hinton, [1968] is shown in Figure 14 (Appendix F).

Some results of calculations of apparent rotational temperatures of the $O_2(b^1\Sigma_g^+)$ (0,1) atmospheric band by other workers, as well as that reported herein, are summarized in Table 6.

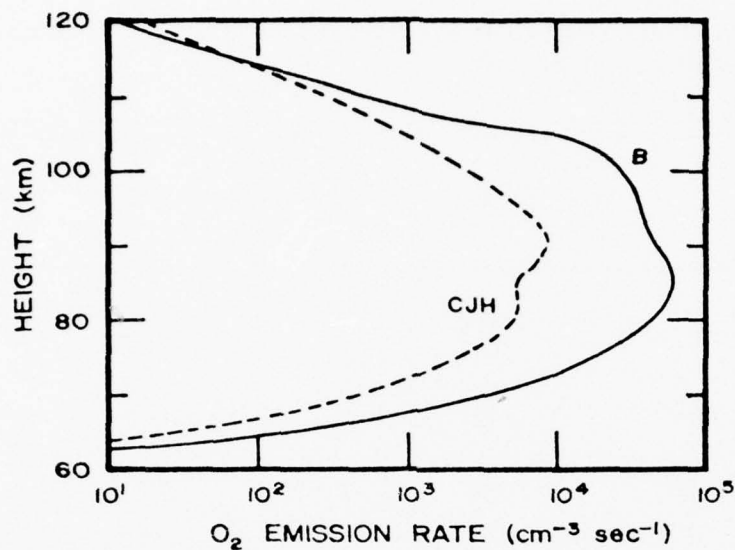


Figure 13. Theoretical volume emission rates for the $O_2(b^1\Sigma_g^+)$ atmospheric (0,1) band night airglow. Curve B is given by Barth [1961]; the curve labeled CJH uses the atomic oxygen distribution of Colegrove et al. [1966].

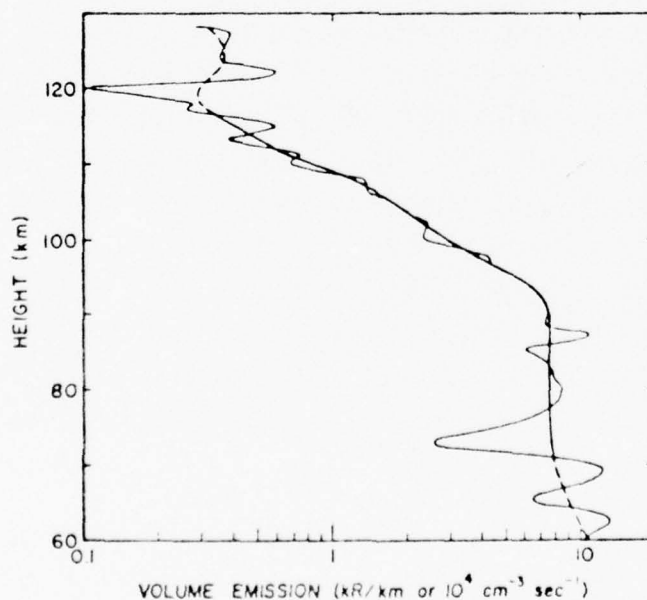


Figure 14. Day airglow volume emission rates profile of the $O_2(b^1\Sigma_g^+)$ atmospheric (0,1) band from rocket borne photometer [Wallace and Hunt, 1968].

Table 6. Rotational temperatures computed from $O_2(b^1\Sigma_g^+)$ atmospheric (0,1) band at 8645 Å.

| Investigators | Season & Year | Latitude | Solar Angle (x) | Condition | Apparent Temperature (°K) |
|---|---------------|----------|------------------------|-------------|------------------------------|
| <i>Meinel</i> [1950] | 1949 | | 43° | Quiet Night | 150 ± 20 |
| <i>Wallace & Chamberlain</i> [1959] | 1959 | | 43° | Aurora | 195 ± 10 |
| <i>Wallace & Chamberlain</i> [1959] | 1959 | | 43° | Quiet Night | 183 ± 7 |
| <i>Sue & Baker</i> [1976] | Spring, 1975 | | 65° | Aurora | 211 ± 10 |

A noticeable apparent correlation between the rotational temperatures of $O_2(b^1\Sigma_g^+)$ band and the radiance of the OH(5,3) band was found in the data taken on March 1, 1975, at Poker Flat, Alaska. Figure 15, which shows the similar pattern of fluctuations. These fluctuations might be due to acoustical gravity waves [Armstrong, 1975], possibly associated with the deposition of energy in the auroral region. The change of intensity and of rotational temperature might be due to the vertical displacement of the emission layer [Baker, 1976]. Further study of these fluctuations would be appropriate.

The strength of the aurora at the time of these $O_2(b^1\Sigma_g^+)$ measurements was ascertained from the radiance of the OI(8446 Å) line which was observed simultaneously. The value of the radiance (Appendix G) of this line was 0.14 kR.

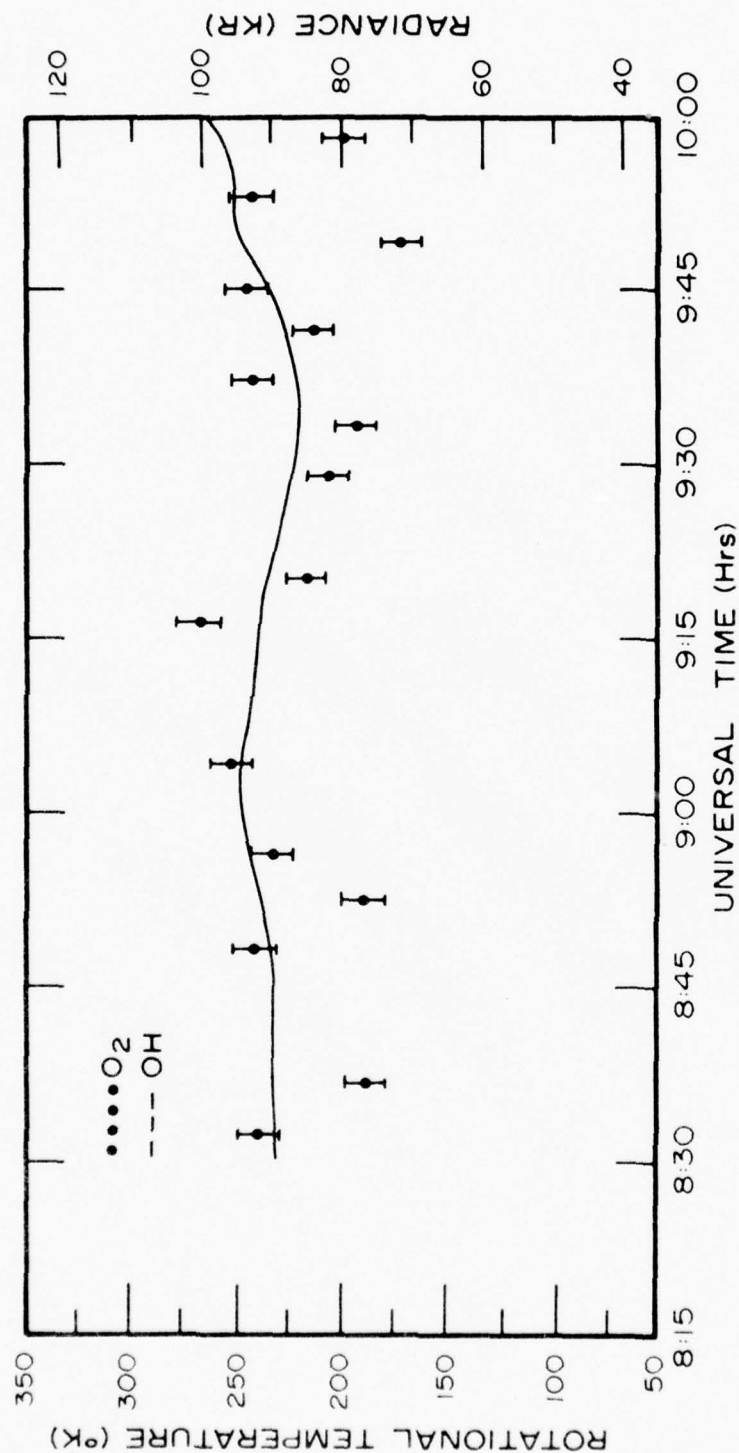


Figure 15. Apparent correlation between the rotational temperature of $O_2(b^1\Sigma_g^+)$ atmospheric (0,1) band and the zenith radiance of the OH(5,3) band observed above Poker Flat, Alaska on March 1, 1975.

CONCLUSIONS AND RECOMMENDATIONS

Conclusions

1. The rotational temperature of the $O_2(b^1\Sigma_g^+)$ atmospheric (0,1) band can be estimated by comparing the band shape of the observed rotational structure with synthetic spectra.
2. A sum of squares weighting method to best fit the observed spectrum with the synthetic spectra appears to be a near optimum procedure.
3. Real typical noise has been added to a synthetic spectrum and used like the real spectrum to analyze the effect of noise. The resulting deviation is much less than that due to the different weighting methods (see Appendix G). The fluctuations of the observed temperature appears to be caused by other factors in addition to noise.
4. The average value of the apparent rotational temperature of $O_2(b^1\Sigma_g^+)$ on March 1, 1975 at 8:45 hrs. UT was 210°K with the band radiance at 1/2 kR.
5. A fluctuation was observed which appears to covary with the intensity of the OH airglow emissions. These may be attributable to atmospheric wave motions.

Recommendations

1. For more accurate values of the spectral line radiances, a curve-fitting technique needs to be developed and applied to the sample points near each line position.
2. The wavenumber spacing between each sample point depends on the position where the wavenumber is located in the spectrum. An interpolation function needs to be developed which will improve the alignment between the observed spectrum and the theoretical spectrum.
3. Establish which part or parts of the band are most sensitive to the rotational temperature changes. By understanding this, the accuracy of the rotational temperature might be able to be improved.
4. Take and analyze data under both quiet and known auroral conditions and also at midlatitude to optimize the model and minimize effects

from contaminating species.

5. Make measurements simultaneous with OH rotational temperature measurements.
6. Develop a noise analysis to better establish the uncertainty of the measurement.
7. Establish the cause of the apparent "wavelike" variations in the temperature and the covariance with OH emissions.
8. The altitude distribution of the $O_2(b^1\Sigma_g^+)$ emission needs to be established under both twilight and nighttime conditions.

REFERENCES

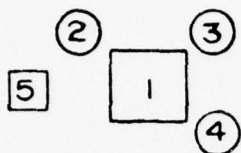
- Armstrong, E.B., The influence of a gravity wave on the airglow hydroxyl rotational temperature at night, *J. Atm. and Terr. Phys.*, **37**, 1585, 1975.
- Babcock, H.D., and L. Herzber, Fine structure of the red system of atmospheric oxygen bands, *Astrophys. J.*, **180**, 167, 1948.
- Baker, D.J., *The Upper-Atmospheric Hydroxyl Airglow*, AFGL/USU, May, 1976.
- Baker, D.J., Field-widened interferometer for Fourier spectroscopy, Chapter 2, *Spectrometric Techniques*, George Vanasse, editor, Academic Press, New York; 1976.
- Barth, C.A., Nitrogen and oxygen atomic reactions in the chemosphere, in Chemical reactions in the Lower and Upper Atmosphere, *Interscience*, 1961.
- Despain, A.M., F.R. Brown Jr., A.J. Steed and D.J. Baker, A large-aperture field-widened interferometer-spectrometer for airglow studies, *Aspen International Conference on Fourier Spectroscopy*, 293, 1970.
- Evans, W.F.J. and E.J. Llewellyn, Molecular oxygen emissions in the airglow, *Ann. Geophys.*, **26**, 167, 1970.
- Herzberg, G., *Molecular Spectra and Molecular Structure*, Prentice-Hall, New York, 1950.
- Krassovsky, V.I., N.N. Shefov and V.I. Yarin, Atlas of the airglow spectrum 3000-12, 400 Å, *Planet Space Sci.* **9**, 890, 1962.
- Meinel, A.B., O₂ emission bands in the infrared spectrum of the night sky, *Astrophys. J.*, **112**, 464, 1950.
- Meinel, A.B., The auroral spectrum from 6200 to 8900 Å, *Astrophys. J.*, **113**, 583, 1951.
- Noxon, J.F., Optical emission from O(¹D) and O₂(^b¹Σ_g⁺) in ultraviolet photolysis of O₂ and CO₂, *J. Chem. Phys.*, **52**, 1852, 1970.
- Noxon, J.F. and A.G. Johanson, Changes in thermospheric molecular oxygen abundance inferred from twilight OI(6300 Å) airglow, *Planet Space Sci.*, **20**, 2125, 1972.
- Noxon J.F., Twilight enhancement in O₂(^b¹Σ_g⁺) airglow emission, *J. Geophys. Res.*, **80**, 1370, 1975.

- Schlapp, R., Fine structure in the $^3\Sigma$ ground state of the oxygen molecule, and the rotational intensity distribution in the atmospheric oxygen band, *Physical Review*, 51, 342, 1936.
- Shimazaki, T. and A.R. Laird., Seasonal effects on distributions of minor neutral constituents in the mesosphere and the lower thermosphere, *Radio Science*, 7, 23, 1971.
- Vallance Jones, A. and Gattinger, R.L., The $O_2(b^1\Sigma_g^+)-(X^3\Sigma_g^-)$ system in aurora, *J. Geophys. Res.*, 79, 4821, 1974.
- Wallace, L. and D.M. Chamberlain, Excitation of O_2 atmospheric bands in the aurora, *Planet Space Sci.*, 2, 60, 1959.
- Wallace, L. and D.M. Hunten, Dayglow of the oxygen A band, *J. Geophys. Res.*, 73, 4813, 1968.
- Whitten R.C. and I.G. Poppoff, *Fundamentals of Aeronomy*, John Wiley & Sons, New York, 1971.

APPENDIX A

NOTATION OF ENERGY STATE OF MOLECULE

The notation of the energy states of a molecule is similar to the notation used for the energy states of an atom. The general form is:



1. A symbol in the position #1 represents the quantum number of the vector component Λ along the internuclear axis of electronic orbital angular momentum L . Its magnitude is $\Lambda(\hbar/2\pi)$, and $\Lambda = 0, 1, 2, 3, \dots, L$. The symbol in position #1 is:
 - Σ when $\Lambda = 0$.
 - Π when $\Lambda = 1$.
 - Δ when $\Lambda = 2$.
 - Φ when $\Lambda = 3$.
 - .
 - .
2. A number in the position #2 is equal to $2S + 1$, S is the quantum number of spin. The value of $2S + 1$ is the spin multiplicity of the energy state.
3. The symbol in the position #3 represents the symmetry of the total eigenfunction of the state with respect to any plane through the internuclear axis. The symmetry is called "+" if the eigenfunctions remain unchanged upon coordinate reflection at the origin. Otherwise it is "-".
4. The symbol in the position #4 represents symmetry of the electronic eigenfunctions. It is "g" if the symmetry property is even. Otherwise it is "u". (From German "gerade" and "ungerade")
5. The symbol in position #5 indicates the excited state by "a", "b", ..., or "A", "B", The ground state is designated by "x".

APPENDIX B
 RELATIVE ABUNDANCE OF $O_2(X^3\Sigma_g^-, v=1)$,
 WITH RESPECT TO TEMPERATURE

Relative abundance of the $v=1$ vibrationally-excited ground state of molecular oxygen, $(X^3\Sigma_g^-, v=1)$, as a function of temperature.

| TEMPERATURE (°K) | RELATIVE ABUNDANCE $[O_2]^*(X^3\Sigma_g^-, v=1)/[O_2](X^3\Sigma_g^-, v=0)$ |
|---------------------|---|
| 160 | 8.382×10^{-7} |
| 170 | 1.909×10^{-6} |
| 180 | 3.968×10^{-6} |
| 190 | 7.635×10^{-6} |
| 200 | 1.376×10^{-5} |
| 210 | 2.345×10^{-5} |
| 220 | 3.807×10^{-5} |
| 230 | 5.926×10^{-5} |
| 240 | 8.890×10^{-5} |
| 250 | 1.291×10^{-4} |
| 260 | 1.822×10^{-4} |
| 270 | 2.506×10^{-4} |
| 280 | 3.370×10^{-4} |
| 290 | 4.440×10^{-4} |
| 300 | 5.742×10^{-4} |

APPENDIX C
THEORETICAL REVIEW

Vibrating Rotator Model

The total energy E of the molecular vibrating rotator model [Herzberg, 1950] is the sum of three component parts; the electronic energy E_e , the vibrational energy E_v , and the rotational energy E_r . That is,

$$E = E_e + E_v + E_r \quad (C.1)$$

or, if we write in the equation in wavenumber units (or term values),

$$T = T_e + G + F \quad (C.2)$$

where:

$$T = \frac{E}{hc}$$

$$T_e = \frac{E_e}{hc}$$

$$G = \frac{E_v}{hc}$$

$$F = \frac{E_r}{hc}$$

h = Planck's constant, 6.625×10^{-27} erg·sec.

c = The velocity of light, 2.99793×10^{10} cm/sec.

The wavenumber of the spectral lines corresponding to the rotations between two electronic states are given by

$$\nu = T' - T'' = (T_e' - T_e'') + (G' - G'') + (F' - F'') \quad (C.3)$$

where the single-primed letters refer to the upper state and the double-primed letters refer to the lower state.

In this paper, consideration is made of the possible transitions between the rotational states for which the vibrational states and

electronic states are given. That is, only the rotational transitions of O_2 from ($^1\Sigma_g^+$, $v=0$) to ($^3\Sigma_g^-$, $v=1$). The first and second terms of Equation (C.3) can be combined into a single term, ν_0 , which is a constant for a specific vibrational transition and is called the band origin. Equation (C.3) can be rewritten as:

$$\nu = \nu_0 + F'(J') - F''(J'') \quad (C.4)$$

where

$F'(J')$ = The rotational term of the upper state.

$F''(J'')$ = The rotational term of the lower state.

J' = The total angular momentum of molecular in upper state.

J'' = The total angular momentum of molecular in lower state.

Hund's Coupling

The different angular momenta in the molecule include the electron spin \vec{S} , electronic orbital angular momentum \vec{L} , and the angular momentum of nuclear rotation \vec{N} . These momenta form a resultant vector \vec{J} which is the total angular momentum of the molecule. In the $^1\Sigma$ state, which is the upper state of the transition resulting in O_2 atmospheric emission band of interest, the spin \vec{S} and the orbital angular momentum \vec{L} of the electrons are zero (refer Appendix A). The angular momentum of nuclear rotation \vec{N} is identical with the total angular momentum \vec{J} . That is,

$$\vec{J} = \vec{S} + \vec{L} + \vec{N} \quad (C.5)$$

if

$$\vec{S} = 0, \vec{L} = 0$$

then

$$\vec{J} = \vec{N}$$

The rotational term of this state can be written as,

$$F(J') = B_v J'(J'+1) - D_v J'^2 (J'+1)^2 + \dots \quad (C.6)$$

where

J' = the total angular momentum of upper level.

$F(J')$ = the rotational term of a state for a given J' .

B_v, D_v = molecular constants, which are listed in Table C.1.

In the $^3\Sigma$ state, which means $\vec{\Lambda} = 0, \vec{S} = 1, \vec{S}$ may be only very weakly coupled to the internuclear axis. This weak coupling of \vec{S} to the internuclear axis is the characteristic of Hund's case (b). If we designate the total angular momentum apart from spin to $\vec{K}, \vec{K} = \vec{N} + \vec{\Lambda}$. The quantum number of \vec{K} can have the integral values;

$$K = \Lambda, \Lambda + 1, \Lambda + 2, \dots \quad (\text{C.7})$$

The quantum number of \vec{J} can have the integral values;

$$J = (K + S), (K + S - 1), (K + S - 2), \dots, |K - S|. \quad (\text{C.8})$$

In the present case for $^3\Sigma$ state, $\Lambda = 0, S = 1$, and Equations (C.7) and (C.8) become

$$K = 0, 1, 2, 3, \dots \quad (\text{C.9})$$

$$J = (1), (0, 1, 2), (1, 2, 3), \dots \quad (\text{C.10})$$

where each group of J 's corresponds to $K = 0, 1, 2, 3, \dots$. The vector diagram of Hund's case (b) is given in Figure C.1. In this figure the nutation of the figure axis, represented by the broken-line ellipse, is much faster than the precessions of \vec{K} and \vec{S} and \vec{J} , represented by the solid-line ellipse. For $\Lambda = 0, \vec{K} (\equiv \vec{N})$ is perpendicular to the internuclear axis.

The rotational terms of each state for a given quantum number K are given by Robert Schlapp, [1936]:

$$F_1(K) = B_v(K+1) + (2K+3) B_v - \lambda - \sqrt{(2K+3)^2 B_v^2 + \lambda^2 - 2\lambda B_v} + \gamma(K+1)$$

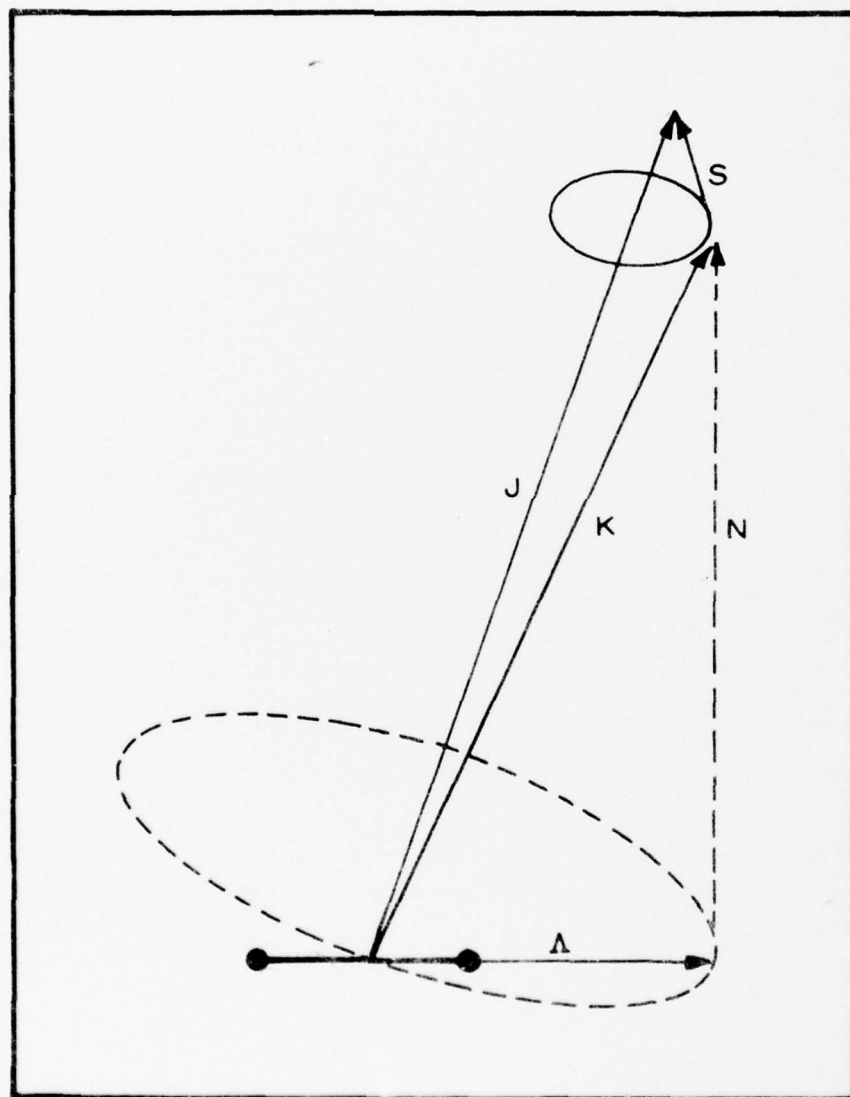


Figure C.1. The vector diagram of Hund's case (b).

$$F_2(K) = B_v K(K+1) - D_v K^2(K+1)^2 \quad (C.11)$$

$$F_3(K) = B_v K(K+1) - (2K-1) B_v \lambda + \sqrt{(2K-1)^2 B_v^2 + \lambda^2 - 2\lambda B_v - \gamma K}$$

where

$F_1(K)$ = the rotational term with $J = K+1$.

$F_2(K)$ = the rotational term with $J = K$.

$F_3(K)$ = the rotational term with $J = K-1$.

B_v, D_v = molecular constants which are listed in Table C.1.

λ, γ = splitting constants which are listed in Table C.1.

Transitions of $O_2(b^1\Sigma_g^+ \rightarrow X^3\Sigma_g^-)$

From quantum mechanical theory, the transition $O_2(b^1\Sigma_g^+ \rightarrow X^3\Sigma_g^-)$ represents a magnetic dipole transition. The selection rules that hold for this type of transition are listed as follows:

- (i) For the quantum number J of the total angular momentum \vec{J}
 $\Delta J = 0, \pm 1$, with the restriction $J = 0 \nleftrightarrow J = 0$.
- (ii) For the quantum number K of the total angular momentum apart from spin, \vec{K}
 $\Delta K = 0, \pm 1$
 and
 $\Delta K = 0$ is forbidden for $\Sigma - \Sigma$ transitions.
- (iii) For magnetic dipole radiation, the rules for the symmetry property are:
 $+ \leftrightarrow +, - \leftrightarrow -, - \leftrightarrow +$
 and
 $g \leftrightarrow g, u \leftrightarrow u, g \leftrightarrow u$

From above selection rules, four branches are possible for each given quantum number K of upper state, $b^1\Sigma_g^+$. They are:

$$(1) Pp(J', K') = F(J', K') - F_2(J'+1, K'+1)$$

Table C.1. Rotational constants of the $X^3\Sigma_g^-$ and $b^1\Sigma_g^+$ states of O_2 .
 [Babcock, 1948]

| Constant | $X^3\Sigma_g^-$ state (cm^{-1}) | $b^1\Sigma_g^+$ state (cm^{-1}) |
|------------|---|---|
| ν_{00} | | 13120.9080 |
| ν_{01} | 1556.3856 | |
| B_0 | 1.43777 ₀ | 1.39132 ₈ |
| B_1 | 1.42197 ₉ | 1.37305 ₄ |
| D_0 | 4.91 ₃ $\times 10$ | 5.40 ₉ $\times 10$ |
| D_1 | 4.82 ₅ $\times 10$ | 5.45 ₈ $\times 10$ |
| λ | 1.984 | |
| γ | -0.00837 | |

The last decimal is printed in full size when the accuracy is well within one unit of the next-to-the-last decimal. If the accuracy is less, the last decimal is a subscript.

- (2) $PQ(J', K') = F(J', K') - F_3(J', K'+1)$
 (3) $RQ(J', K') = F(J', K') - F_1(J', K'-1)$
 (4) $RR(J', K') = F(J', K') - F_2(J'-1, K'-1)$

where J' , K' refer to the quantum numbers of the upper level.

The superscripts represent the changes of quantum number K when the capital letters represent the changes of quantum number J . P represents the quantum number increased by 1. Q represents equal and R represents the quantum number decreased by 1 when the transition takes place from one state to another.

By substituting Equation (C.11) into (C.12), the vibrational term values $F''(J'')$ of the lower state, $X^3\Sigma_g^-$ are obtained. From Equation (C.4) and (C.6) the wavelength of each transition which corresponds each line of transition from $b^1\Sigma_g^-$ to $X^3\Sigma_g^-$ shown in Figure C.2 can be obtained. In Figure C.2, the states represented by broken circles are absent because of zero nuclear spin. The wavenumbers corresponding to the lines in Figure C.2 are generated by computer and are listed in Table C.2.

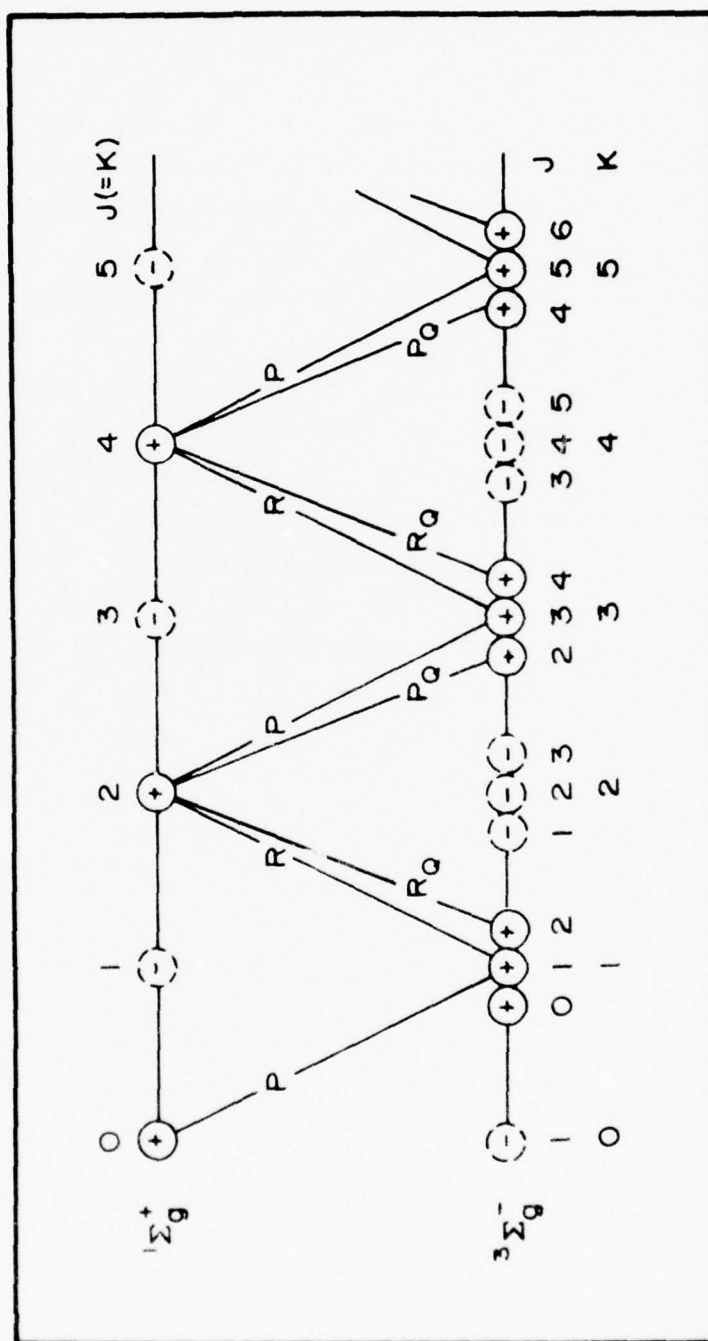


Figure C.2. Transition between $1\Sigma_g^+$ and $3\Sigma_g^-$.

Table C.2. Wavenumbers (cm^{-1}) of lines in (0-1) band of $\text{O}_2(^1\Sigma-^3\Sigma)$.

| K' | R_R Branch | R_Q Branch | P_Q Branch | Branch |
|------|-----------------|-----------------|-----------------|-----------|
| 0 | | | | 11561.678 |
| 2 | 11570.026 | 11571.906 | 11557.887 | 11555.807 |
| 4 | 11575.283 | 11577.234 | 11551.701 | 11549.691 |
| 6 | 11580.293 | 11582.281 | 11545.304 | 11543.333 |
| 8 | 11585.054 | 11587.069 | 11538.675 | 11536.731 |
| 10 | 11589.564 | 11591.603 | 11531.806 | 11529.885 |
| 12 | 11593.821 | 11595.881 | 11524.697 | 11522.797 |
| 14 | 11597.823 | 11599.903 | 11517.345 | 11515.466 |
| 16 | 11601.567 | 11603.667 | 11509.750 | 11507.890 |
| 18 | 11605.051 | 11607.169 | 11501.911 | 11500.070 |
| 20 | 11608.273 | 11610.410 | 11493.827 | 11492.004 |
| 22 | 11611.228 | 11613.383 | 11485.495 | 11483.690 |
| 24 | 11613.914 | 11616.087 | 11476.916 | 11475.129 |
| 26 | 11616.328 | 11618.518 | 11468.086 | 11466.317 |
| 28 | 11618.464 | 11620.673 | 11459.006 | 11457.253 |
| 30 | 11620.321 | 11622.547 | 11449.670 | 11447.936 |

Program 02EMI

```

*11: 001171
1      THIS PROGRAM COMPUTES ATMOSPHERIC BOND* (SIGMA SINGLE)
      *1166* TRIPLET* 1 BOND*
C***** THIS PROGRAM BOND IS 0.101*
      DIMENSION K(4),EKK(4),DIF(100),AINT(100),KINT(100)
      BOF=1.391328
      RIFF=1.421979
      DOF=5.395E-6
      DUFF=4.825E-6
      XLMDS=1.984
      GAMS=0.00837
      V01=11564.5222
      H=8.825E-27
      DK=1.30044E-16
      C=2.99793E+10
      T=1975.0
      CT=H*(100/((DK*1)
      XT=XLMDS**2-2.0*XLMDS*RIFF
      WRITE(1,301)
301    FORMAT(4X,'NN',/,'KEY',/,'JEP',/,'JEP',/,'NAME',/,'X',
1      /,'M OF TRANS',/,'X',/,'ABS. INTENSITY')
      QR=0.0
      DO 110 N=1,20
      KF=J*(N-1)
      JE=KE
      EJE=JE
      DSTR=EXP(-BOF*EJ*(EJ+1.0)*CT)
      HFF=(2.0*EJE+1.0)*DSTR
      QR=QR+TERM
110    CONTINUE
      K(1)=1
      K(2)=1
      K(3)=1
      K(4)=1
      EKK(1)=*KK*
      EKK(2)=*KK*
      EKK(3)=*EQ*
      EKK(4)=*FF*
      NN=0
      DO 350 N=1,20
      NF=2*(N-1)
      T=(NF-0.20)/10.20
350    NN=NN+1
      M=4
      JE=KE
      EK=KE
      EJE=JE
      BV=BOF
      DV=DOF
      EJS=DV*EK*(EK+1.0)/DV*(EJE**2*(EK+1.0)**2
      DSTR=EXP(-DV*JE*(EJ+1.0)*CT)
      SJE=(EJ+2.0)/2.0
      KFF=KE+1
      JFF=KEF
      EK=KEF
      BV=KEFF
      DV=DIEF
      EJS=DV*EK*(EK+1.0)/DV*(EJE**2*(EK+1.0)**2
      DSTR=EXP(-DV*JE*(EJ+1.0)*CT)
      BV=DIEF
      DO 250 M=1,4
      EJE=KE+K(1)*H
      DV=DIEF
      EK=KEF
      Q2=DV*EK*(EK+1.0)/DV*(EJE**2*(EK+1.0)**2
      GO TO (30,40,30,40)M
30    EJE=KE
      SJE=(EJ+1.0)/2.0
      BV=KEF

```

BEST AVAILABLE COPY

```

      I=J
      BV=BOF
      DV=DOF
      FSS=BV*FK*(FK+1.0)-DV*FK**2*(FK+1.0)**2
      DSTREXFC(-BV*FJ*(FJ+1.0)*ET)
      SJ=(FJ+2.0)/2.0
      KFF=KFF+1
      JFF=JFF
      FK=KFF
      RV=RIFF
      DV=DIFF
      FST=DV*FK*(FK+1.0)-DV*FK**2*(FK+1.0)**2
      DIFF(NN)=FSS-FST+V01
      AINT(NN)=(DIFF(NN)**3*SJ*DSTR)/QR
      WRITE(1,302)NN,IF,JF,KFF,JFF,PQR(M),DIFF(NN),AINT(NN)
      GO TO 220
20    JF=KF
      FK=KF
      FJ=JP
      BV=BOF
      DV=DOF
      FSS=BV*FK*(FK+1.0)-DV*FK**2*(FK+1.0)**2
      DSTREXFC(-BV*FJ*(FJ+1.0)*ET)
      RV=RIFF
      DO 220 M=1,4
      KFF=KFF+1(M)
      DV=DIFF
      FK=KF
      X2=DV*FK*(FK+1.0)-DV*FK**2*(FK+1.0)**2
      GO TO (30,40,50,60)M
30    FST=X2
      SJ=(FJ+1.0)/2.0
      JFF=KFF
      GO TO 100
40    X3=(2.0*FK+3.0)*BV
      FST=X2+X3-X1*MDA+SORT(X3**2+X1)+GAMA*(FK+1.0)
      SJ=(FJ+1.0/4.0)/2.0
      JFF=KFF+1
      GO TO 100
50    X4=(2.0*FK-1.0)*BV
      FST=X2-X4-X1*MDA+SORT(X4**2+X1)-GAMA*FK
      SJ=(FJ+3.0/4.0)/2.0
      JFF=KFF-1
      GO TO 100
60    FST=X2
      SJ=(FJ+2.0)/2.0
      JFF=KFF
      GO TO 100
100   NN=NN+1
      DIFF(NN)=FSS-FST+V01
      AINT(NN)=(DIFF(NN)**3*SJ*DSTR)/QR
      WRITE(1,302)NN,KF,JF,KFF,JFF,PQR(M),DIFF(NN),AINT(NN)
302   FORMAT(1X,SI4,2X,A2,2X,F14.5,2X,E14.6)
220   CONTINUE
330   CONTINUE
      TINT=0.0
      DO 440 NN=1,77
      TINT=TINT+AINT(NN)
440   CONTINUE
      WRITE(1,303)T
      SKINT=0.0
      DO 550 NN=1,77
      RINT(NN)=(AINT(NN)*1000.0)/TINT
      WRITE(1,304)NN,DIFF(NN),RINT(NN)
      SKINT=SKINT+RINT(NN)
550   CONTINUE
      CALL DDOPEN('SYS',D1951)
      WRITE(4,309)(J,DIFF(J),RINT(J),J=1,77)
      CALL DDCLSE
309   FORMAT(14,2X,F14.6,2X,F14.6)
C***** WRITE OUTPUT DATA FILE NAME *****
303   FORMAT(//,1X,THE FOLLOWING DATA IS STORED IN 'D1951'//
1     1X,THE TEMPERATURE=F13.2//
1     2X,NN,4X,V OF TRANS,2X,REL. INTENSITY)
304   FORMAT(14,2X,F14.5,2X,F14.5)
      WRITE(1,305)SKINT
305   FORMAT(1X,THE TOTAL INTENSITY=F13.5)
      CALL EXIT
      END

```

Output of Program 02EMI

R. FORT
*02EMI 02EMI/0/G

| NN | KF | JF | KFF | JFF | NAME | V OF TRANS. | ABS. INTENSITY |
|----|----|----|-----|-----|------|-------------|----------------|
| 1 | 0 | 0 | 1 | 1 | FF | 11561.67834 | 0.316221E+11 |
| 2 | 2 | 2 | 1 | 1 | RR | 11570.02598 | 0.148988E+11 |
| 3 | 2 | 2 | 1 | 2 | RQ | 11571.90576 | 0.335387E+11 |
| 4 | 2 | 2 | 3 | 2 | FQ | 11557.88674 | 0.408429E+11 |
| 5 | 2 | 2 | 3 | 3 | FF | 11555.80654 | 0.593758E+11 |
| 6 | 4 | 4 | 3 | 3 | RR | 11575.28311 | 0.387458E+11 |
| 7 | 4 | 4 | 3 | 4 | RQ | 11577.23367 | 0.549459E+11 |
| 8 | 4 | 4 | 5 | 4 | FQ | 11551.70053 | 0.610048E+11 |
| 9 | 4 | 4 | 5 | 5 | FF | 11549.69111 | 0.770184E+11 |
| 10 | 6 | 6 | 5 | 5 | RR | 11580.29288 | 0.516153E+11 |
| 11 | 6 | 6 | 5 | 6 | RQ | 11582.28069 | 0.645524E+11 |
| 12 | 6 | 6 | 7 | 6 | FQ | 11545.30470 | 0.690510E+11 |
| 13 | 6 | 6 | 7 | 7 | FF | 11543.33278 | 0.817982E+11 |
| 14 | 8 | 8 | 7 | 7 | RR | 11585.05380 | 0.531732E+11 |
| 15 | 8 | 8 | 7 | 8 | RQ | 11587.06918 | 0.627012E+11 |
| 16 | 8 | 8 | 9 | 8 | FQ | 11538.67468 | 0.656715E+11 |
| 17 | 8 | 8 | 9 | 9 | FF | 11536.73082 | 0.750152E+11 |
| 18 | 10 | 10 | 9 | 9 | RR | 11589.56363 | 0.463371E+11 |
| 19 | 10 | 10 | 9 | 10 | RQ | 11591.60286 | 0.528007E+11 |
| 20 | 10 | 10 | 11 | 10 | FQ | 11531.80599 | 0.545238E+11 |
| 21 | 10 | 10 | 11 | 11 | FF | 11529.88523 | 0.608334E+11 |
| 22 | 12 | 12 | 11 | 11 | RR | 11593.82089 | 0.353571E+11 |
| 23 | 12 | 12 | 11 | 12 | RQ | 11595.88098 | 0.393959E+11 |
| 24 | 12 | 12 | 13 | 12 | FQ | 11524.69664 | 0.402534E+11 |
| 25 | 12 | 12 | 13 | 13 | FF | 11522.79749 | 0.441780E+11 |
| 26 | 14 | 14 | 13 | 13 | RR | 11597.82260 | 0.240286E+11 |
| 27 | 14 | 14 | 13 | 14 | RQ | 11599.90280 | 0.263532E+11 |
| 28 | 14 | 14 | 15 | 14 | FQ | 11517.34516 | 0.266796E+11 |
| 29 | 14 | 14 | 15 | 15 | FF | 11515.46612 | 0.289481E+11 |
| 30 | 16 | 16 | 15 | 15 | RR | 11601.56652 | 0.146853E+11 |
| 31 | 16 | 16 | 15 | 16 | RQ | 11603.66684 | 0.159177E+11 |
| 32 | 16 | 16 | 17 | 16 | FQ | 11509.75003 | 0.160123E+11 |
| 33 | 16 | 16 | 17 | 17 | FF | 11507.89037 | 0.171989E+11 |
| 34 | 18 | 18 | 17 | 17 | RR | 11605.05115 | 0.811990E+10 |
| 35 | 18 | 18 | 17 | 18 | RQ | 11607.16935 | 0.722172E+10 |
| 36 | 18 | 18 | 19 | 18 | FQ | 11501.91128 | 0.871910E+10 |
| 37 | 18 | 18 | 19 | 19 | FF | 11500.07024 | 0.929591E+10 |
| 38 | 20 | 20 | 19 | 19 | RR | 11608.27279 | 0.407821E+10 |
| 39 | 20 | 20 | 19 | 20 | RQ | 11610.40961 | 0.434891E+10 |
| 40 | 20 | 20 | 21 | 20 | FQ | 11493.82665 | 0.432340E+10 |
| 41 | 20 | 20 | 21 | 21 | FF | 11492.00350 | 0.458166E+10 |
| 42 | 22 | 22 | 21 | 21 | RR | 11611.22769 | 0.186575E+10 |
| 43 | 22 | 22 | 21 | 22 | RQ | 11613.38314 | 0.197791E+10 |
| 44 | 22 | 22 | 23 | 22 | FQ | 11485.49541 | 0.195628E+10 |
| 45 | 22 | 22 | 23 | 23 | FF | 11483.69014 | 0.208279E+10 |
| 46 | 24 | 24 | 23 | 23 | RR | 11613.91437 | 0.779082E+09 |
| 47 | 24 | 24 | 23 | 24 | RQ | 11616.08595 | 0.821885E+09 |
| 48 | 24 | 24 | 25 | 24 | FQ | 11476.91607 | 0.809041E+09 |
| 49 | 24 | 24 | 25 | 25 | FF | 11475.12863 | 0.849204E+09 |
| 50 | 26 | 26 | 25 | 25 | RR | 11616.32761 | 0.297386E+09 |
| 51 | 26 | 26 | 25 | 26 | RQ | 11618.51808 | 0.312431E+09 |
| 52 | 26 | 26 | 27 | 26 | FQ | 11468.08649 | 0.306175E+09 |
| 53 | 26 | 26 | 27 | 27 | FF | 11466.31687 | 0.420334E+09 |
| 54 | 28 | 28 | 27 | 27 | RR | 11618.46444 | 0.103889E+09 |
| 55 | 28 | 28 | 27 | 28 | RQ | 11620.67279 | 0.108761E+09 |
| 56 | 28 | 28 | 29 | 28 | FQ | 11459.00583 | 0.106130E+09 |
| 57 | 28 | 28 | 29 | 29 | FF | 11457.25324 | 0.110394E+09 |
| 58 | 30 | 30 | 29 | 29 | RR | 11620.32112 | 0.332468E+08 |
| 59 | 30 | 30 | 29 | 30 | RQ | 11622.54581 | 0.446805E+08 |
| 60 | 30 | 30 | 31 | 30 | FQ | 11449.67004 | 0.337214E+08 |
| 61 | 30 | 30 | 31 | 31 | FF | 11447.93555 | 0.350782E+08 |
| 62 | 32 | 32 | 31 | 31 | RR | 11621.89339 | 0.975077E+07 |
| 63 | 32 | 32 | 31 | 32 | RQ | 11624.13887 | 0.101519E+08 |
| 64 | 32 | 32 | 33 | 32 | FQ | 11440.07891 | 0.982730E+07 |
| 65 | 32 | 32 | 33 | 33 | FF | 11438.36155 | 0.101578E+08 |
| 66 | 34 | 34 | 33 | 33 | RR | 11623.17618 | 0.262429E+07 |
| 67 | 34 | 34 | 33 | 34 | RQ | 11625.45594 | 0.273529E+07 |
| 68 | 34 | 34 | 35 | 34 | FQ | 11430.22974 | 0.282911E+07 |
| 69 | 34 | 34 | 35 | 35 | FF | 11428.50290 | 0.272142E+07 |
| 70 | 36 | 36 | 35 | 35 | RR | 11624.16562 | 0.648056E+06 |
| 71 | 36 | 36 | 35 | 36 | RQ | 11626.44257 | 0.671574E+06 |
| 72 | 36 | 36 | 37 | 36 | FQ | 11420.11731 | 0.646750E+06 |
| 73 | 36 | 36 | 37 | 37 | FF | 11418.43473 | 0.666802E+06 |
| 74 | 38 | 38 | 37 | 37 | RR | 11624.05629 | 0.142719E+06 |
| 75 | 38 | 38 | 37 | 38 | RQ | 11626.15110 | 0.151968E+06 |
| 76 | 38 | 38 | 39 | 38 | FQ | 11409.74009 | 0.145191E+06 |
| 77 | 38 | 38 | 39 | 39 | FF | 11408.07567 | 0.150108E+06 |

BEST AVAILABLE COPY

THE FOLLOWING DATA IS STORED IN #D1951*
 THE TEMPERATURE= 195.00

NN W OF TRANS. REL. INTENSITY
 1 11561.67834 20.47694
 2 11570.02598 9.64774
 3 11571.90576 21.71800
 4 11557.88674 26.44787
 5 11555.80654 38.44886
 6 11575.28311 25.10283
 7 11577.23367 35.58032
 8 11551.70053 39.50371
 9 11549.69111 49.87339
 10 11580.29288 33.42356
 11 11582.28069 41.80096
 12 11545.30420 44.71404
 13 11543.33278 52.96727
 14 11585.05380 34.43240
 15 11587.06918 40.60222
 16 11538.67468 42.52564
 17 11536.73082 48.57617
 18 11589.56363 30.00568
 19 11591.60286 34.19118
 20 11531.80599 35.30695
 21 11529.88523 39.39272
 22 11593.82089 22.89552
 23 11595.88098 25.51088
 24 11524.69664 26.06614
 25 11522.79749 28.60750
 26 11597.82260 15.55975
 27 11599.90280 17.06506
 28 11517.34516 17.28937
 29 11515.46612 18.74539
 30 11601.56652 9.50948
 31 11603.66684 10.30753
 32 11509.75003 10.36879
 33 11507.89037 11.13718
 34 11605.05115 5.25805
 35 11607.16935 5.64776
 36 11501.91128 5.64607
 37 11500.07024 8.01958
 38 11608.27279 2.64085
 39 11610.40961 2.81615
 40 11493.82665 2.75962
 41 11492.00350 2.96686
 42 11611.22769 1.20817
 43 11613.38314 1.28080
 44 11485.49541 1.26679
 45 11483.69014 1.33576
 46 11613.91437 0.50450
 47 11616.08695 0.53221
 48 11476.91607 0.52390
 49 11475.12868 0.55010
 50 11616.32761 0.19257
 51 11618.51808 0.20232
 52 11468.08639 0.19826
 53 11466.31687 0.20743
 54 11618.46444 0.06727
 55 11620.67279 0.07043
 56 11459.00562 0.06872
 57 11457.25324 0.07168
 58 11620.32112 0.02153
 59 11622.54661 0.02247
 60 11449.67004 0.02184
 61 11447.93555 0.02271
 62 11621.89319 0.00632
 63 11624.13582 0.00657
 64 11440.07891 0.00636
 65 11438.36155 0.00660
 66 11623.17618 0.00170
 67 11625.43594 0.00176
 68 11430.22924 0.00170
 69 11428.92902 0.00176
 70 11624.16562 0.00042
 71 11626.44252 0.00043
 72 11470.11731 0.00042
 73 11418.43423 0.00043
 74 11624.85629 0.00010
 75 11627.15107 0.00010
 76 11409.74089 0.00009
 77 11408.07569 0.00010
 THE TOTAL INTENSITY= 1000.00008

BEST AVAILABLE COPY

Program SORT

```

R PIF
*TTY: SORT/T
C      ***THIS PROGRAM SORT DATA IN AN INCREASING ORDER
      DIMENSION NO(100),DIFF(100),RINT(100)
C      ***INPUT DATA *****
      CALL IOFEN('SYS','D2351')
      K=1
35     READ(4,304)N,U,R
      NO(K)=N
      DIFF(K)=D
      RINT(K)=R
10     K=K+1
      IF(K-77)35,35,31
31     K=K-1
      M=K
70     FM=M
      M=IFIX(FM/2.0)
      IF(M)180,333,180
180    IK=K-M
      I=1
110   L=I
120   J=L+M
      IF(DIFF(L)-DIFF(J))190,190,240
240   T1=DIFF(L)
      T2=RINT(L)
      IT=NO(L)
      DIFF(L)=DIFF(J)
      RINT(L)=RINT(J)
      NO(L)=NO(J)
      DIFF(J)=T1
      RINT(J)=T2
      NO(J)=IT
      L=L-M
      IF(L)190,190,120
190   I=I+1
      IF(I-IK)110,110,70
333   CONTINUE
      WRITE(1,733)
733   FORMAT(1X,'TEMPERATURE=195 K',1X,'THE DATA ARE STORED IN
1     *D1952*')
1     1X,'N',2X,'INDEX',4X,'WAVE NO.',5X,'RINT')
C      ***OUTPUT DATA ***
      CALL IOFEN('SYS','D2352')
      DO 777 I=1,77
      WRITE(4,734)DIFF(I),RINT(I)
734   FORMAT(2A6)
      WRITE(1,735)I,NO(I),DIFF(I),RINT(I)
735   FORMAT(I3,T4,F14.5,F14.5)
777   CONTINUE
      CALL OCLOSE
304   FORMAT(I4,2X,F14.6,2X,F14.6)
      CALL EXIT
      END

```

BEST AVAILABLE COPY

Output of Program SORT

| N | INDEX | WAVE NO. | RINT |
|----|-------|-------------|----------|
| 1 | 77 | 11408.07569 | 0.00107 |
| 2 | 76 | 11409.74089 | 0.00104 |
| 3 | 73 | 11418.43348 | 0.00368 |
| 4 | 72 | 11420.11657 | 0.00356 |
| 5 | 69 | 11428.52902 | 0.01171 |
| 6 | 68 | 11430.22924 | 0.01130 |
| 7 | 65 | 11438.36155 | 0.03471 |
| 8 | 64 | 11440.07891 | 0.03345 |
| 9 | 61 | 11447.93480 | 0.09579 |
| 10 | 60 | 11449.67004 | 0.09209 |
| 11 | 57 | 11457.25324 | 0.24597 |
| 12 | 56 | 11459.00562 | 0.23583 |
| 13 | 53 | 11466.31613 | 0.58733 |
| 14 | 52 | 11468.08564 | 0.56137 |
| 15 | 49 | 11475.12868 | 1.30330 |
| 16 | 48 | 11476.91532 | 1.24122 |
| 17 | 45 | 11483.69014 | 2.68535 |
| 18 | 44 | 11485.49467 | 2.54669 |
| 19 | 41 | 11492.00350 | 5.13224 |
| 20 | 40 | 11493.82665 | 4.84293 |
| 21 | 37 | 11500.07024 | 9.08624 |
| 22 | 36 | 11501.91128 | 8.52244 |
| 23 | 33 | 11507.89037 | 14.87556 |
| 24 | 32 | 11509.75003 | 13.84924 |
| 25 | 29 | 11515.46537 | 22.46691 |
| 26 | 28 | 11517.34516 | 20.72182 |
| 27 | 25 | 11522.79675 | 31.19969 |
| 28 | 24 | 11524.69664 | 28.42806 |
| 29 | 21 | 11529.88523 | 39.64413 |
| 30 | 20 | 11531.80524 | 35.53228 |
| 31 | 17 | 11536.73082 | 45.74563 |
| 32 | 16 | 11538.67393 | 40.04766 |
| 33 | 13 | 11543.33204 | 47.33344 |
| 34 | 12 | 11545.30420 | 39.95806 |
| 35 | 9 | 11549.69036 | 42.88787 |
| 36 | 8 | 11551.69978 | 33.97062 |
| 37 | 5 | 11555.80654 | 32.26451 |
| 38 | 4 | 11557.88674 | 22.19383 |
| 39 | 1 | 11561.67834 | 17.00409 |
| 40 | 2 | 11570.02598 | 8.09594 |
| 41 | 3 | 11571.90576 | 18.22474 |
| 42 | 6 | 11575.28236 | 21.58680 |
| 43 | 7 | 11577.23292 | 30.59676 |
| 44 | 10 | 11580.29213 | 29.86848 |
| 45 | 11 | 11582.27995 | 37.35483 |
| 46 | 14 | 11585.05305 | 32.42601 |
| 47 | 15 | 11587.06918 | 38.23632 |
| 48 | 18 | 11589.56363 | 30.19718 |
| 49 | 19 | 11591.60286 | 34.40939 |
| 50 | 22 | 11593.82015 | 24.97013 |
| 51 | 23 | 11595.88098 | 27.82248 |
| 52 | 26 | 11597.82260 | 18.64883 |
| 53 | 27 | 11599.90280 | 20.45298 |
| 54 | 30 | 11601.56652 | 12.70149 |
| 55 | 31 | 11603.66684 | 13.76742 |
| 56 | 34 | 11605.05041 | 7.93675 |
| 57 | 35 | 11607.16861 | 8.52501 |
| 58 | 38 | 11608.27279 | 4.56828 |
| 59 | 39 | 11610.40961 | 4.87152 |
| 60 | 42 | 11611.22769 | 2.42804 |
| 61 | 43 | 11613.38239 | 2.57485 |
| 62 | 46 | 11613.91362 | 1.19524 |

| | | | |
|----|----|-------------|---------|
| 63 | 47 | 11616.08621 | 1.26092 |
| 64 | 50 | 11616.32761 | 0.54526 |
| 65 | 54 | 11618.46444 | 0.23085 |
| 66 | 51 | 11618.51808 | 0.57284 |
| 67 | 58 | 11620.32037 | 0.09079 |
| 68 | 55 | 11620.67204 | 0.24167 |
| 69 | 62 | 11621.89319 | 0.03319 |
| 70 | 59 | 11622.54661 | 0.09476 |
| 71 | 66 | 11623.17618 | 0.01129 |
| 72 | 63 | 11624.13507 | 0.03453 |
| 73 | 70 | 11624.16562 | 0.00357 |
| 74 | 74 | 11624.85629 | 0.00105 |
| 75 | 67 | 11625.43520 | 0.01172 |
| 76 | 71 | 11626.44252 | 0.00370 |
| 77 | 75 | 11627.15107 | 0.00109 |

Program CNVLS

```

*ITY:CNVLS/T
C      ///THIS PROGRAM CONVOLVE THE INPUT DATA BY A RESOLUTION=RES CM-1
C      ///OUTPUT DATA FORMAT (I,SUM)--(I,INTENSITY)--(A2,A6)
C      ///INPUT DATA DIMENSION
      DIMENSION WNN(77),RINTT(77)
      CALL IOFEN('SYS','D1952')
      K=77
      DO 11 I=1,K
      READ(4,202)WNN(I),RINTT(I)
202    FORMAT(2A6)
      11 CONTINUE
C      ///THE WAVENUMBER CORRESPOND TO ORIGIN
      W=11400.0
C      ///OUTPUT DATA FILE
      CALL ODFEN('SYS','D1953')
C      ///RESOLUTION=RES CM-1
C      ///INTERVAL OF ONE SIDE= RES*4.0
      RES=3.0
      DINT=RES*4.0
      JB=1
C      ///THE UPPER NUMBER OF DO LOOP IS THE NUMBER OF OUTPUT POINTS
      DO 110 I=1,500
      W=W+0.5
      SUM=0.0
      J=JB
      N=0
      3    DWN=WNN(J)-W
          IF(DWN)5,30,15
      5    IF(DWN+DINT)10,25,25
      10   J=J+1
          GO TO 3
      25   N=N+1
          IF(N-1)30,26,30
      26   JB=J
          GO TO 30
      15   IF(DWN-DINT)30,30,60
      30   X=DWN*3.1416/RES
          RINT=RINTT(J)
          AX=ABS(X)
          IF(AX-0.000001)40,40,50
      40   RATIO=1.0
          GO TO 55
      50   RATIO=SIN(X)/X
      55   SUM=SUM+RINT*RATIO*(1.0-(DWN/DINT)**2)**2
          IF(J-K)10,60,60
      60   IF(SUM)70,80,80
      70   SUM=0.0
      80   WRITE(4,320)I,SUM
      320  FORMAT(A2,A6)
      110  CONTINUE
          CALL OCLOSE
          CALL EXIT
          END

```

Program DTPRS

```

*SYS:DTPRS<MTB;\;\:DTPRS/A
*TTY:<DTPRS/T
      DIMENSION WNN(70),RINTT(70),R(70)
      READ(1,202)N,FLNAME
202  FORMAT('READ FILE NO. =',I2/'OUTPUT FILE NAME =',A6)
      KC=2047+1
      CALL DISK(0,60,0,20,0,-KC,ISR)
      WRITE(1,910)
910  FORMAT('CHECK')
      IAD=-280
      DO 11 I=1,70
      CALL DATAS(0,2,IAD,IVAL)
      XF=IVAL
      IAD=IAD+1
      CALL DATAS(0,2,IAD,IVAL)
      XMAN=IVAL
      RINTT(I)=XMAN*(2.0**XF)
      IAD=IAD+3
11  CONTINUE
      WRITE(1,340)(I,RINTT(I),I=1,6)
340  FORMAT(2(4X,I2,E16.6))
C    ///INSTRUMENTAL RESPONSE CORRECTION AND NORMALIZATION
C    ///SET THE START DATA POINT
      ISTR=29
      DMINI=0.0
C    ///'DAIR' IS THE FILE FOR INSTRUMENTAL RESPONSE
      CALL IOFEN('SYS','DAIR')
      READ(4,302)(R(I),I=1,40)
302  FORMAT(F5.3)
      DO 44 I=41,70
      R(I)=1.00
44  CONTINUE
      TOTL=0.0
      DO 33 I=ISTR,70
      RINTT(I)=RINTT(I)-DMINI
      RINTT(I)=RINTT(I)/R(I)
      TOTL=TOTL+RINTT(I)
33  CONTINUE
      IEND=70-ISTR+1
      DO 22 I=1,IEND
      N=I+ISTR-1
      RINTT(I)=(RINTT(N)*1000.0)/TOTL
      FN=N
      WNN(I)=11457.46+FN*2.23
22  CONTINUE
      WRITE(1,360)(I,WNN(I),RINTT(I),I=1,6)
360  FORMAT(I3,3X,F10.2,3X,E12.4)
C    ///CONVOLVE THE DATA BY A RESOLUTION=RES CM-1
      WRITE(1,910)
C    ///SET K=THE NO. OF LINES OF LINE SPECTRUM
      K=42
C    ///THE WAVENUMBER CORRESPOND TO ORIGIN
      W=11400.0
C    ///OUTPUT DATA FILE
      CALL OOFEN('SYS',FLNAME)
C    ///RESOLUTION=RES CM-1
C    ///INTERVAL OF ONE SIDE= RES*4.0
      RES=3.0
      DINT=RES*4.0
      JB=1
C    ///THE UPPER NUMBER OF DO LOOP IS THE NUMBER OF OUTPUT POINTS
      DO 110 I=1,500
      W=W+0.5
      SUM=0.0
      J=JB
      N=0

```

```

3   DWN=WNN(J)-W
   IF(DWN)5,30,15
5   IF(DWN+DINT)10,25,25
10  J=J+1
   GO TO 3
25  N=N+1
   IF(N-1)30,26,30
26  JB=J
   GO TO 30
15  IF(DWN-DINT)30,30,60
30  X=DWN*3.1416/RES
   RINT=RINT(J)
   AX=ABS(X)
   IF(AX-0.000001)40,40,50
40  RATIO=1.0
   GO TO 55
50  RATIO=SIN(X)/X
55  SUM=SUM+RINT*RATIO*(1.0-(DWN/DINT)**2)**2
   IF(J-K)10,60,60
60  IF(SUM)70,80,80
70  SUM=0.0
80  WRITE(4,320)I,SUM
320 FORMAT(A2,A6)
110 CONTINUE
   CALL OCLOSE
   CALL EXIT
   END

```

Program CMPR

BEST AVAILABLE COPY

```

R PIP
*IIY:CMPIR/I
C      ***THIS PROGRAM COMPARE THE DATA SPECTRUM WITH SYNTHETIC SPECTRUM
      DIMENSION RINT(500)*D(500)
      RES=3.00
C      ***READ SYNTHETIC VALUE
      READ(1,1)I,FLNAME
      1  FORMAT('TEMPERATURE= ',F5.1//INPUT SYNTHETIC DATA FILE= ',A6)
      CALL IOFEN('SYS',FLNAME)
      READ(4,202)(IUN,RINT(I),I=1,500)
      202  FORMAT(A2,A5)
C      ***READ THE MEASUREMENTAL DATA
      READ(1,2)N,FLDATA
      2  FORMAT('ORIGINAL FILE NO. =',I2//DATA FILE NAME =',A6)
      CALL IOFEN('SYS',FLDATA)
      READ(4,202)(IUN,D(I),I=1,500)
C      ***SET START POINT AND END POINT
      STR=(11539.34-11400.0)/0.5
      ISTR=STR
      END=((11457.46+70.0*2.23)-11400.0)/0.5
      IEND=END
C      ***SCALING THE SYNTHETIC SPECTRUM TO MATCH DATA
      SMSN=0.0
      SMNT=0.0
      DO 22 I=ISTR,IEND
      SMSN=SMSN+RINT(I)*0.5
      SMNT=SMNT+D(I)*0.5
      22  CONTINUE
      RATIO=SMNT/SMSN
      DO 33 I=ISTR,IEND
      RINT(I)=RINT(I)*RATIO
      33  CONTINUE
C      ***CALCULATE THE DEVIATION OF THE SYNTHETIC SPECTRUM WITH DATA
      SUM=0.0
      SD=0.0
      WTAD=0.0
      SSQ=0.0
      DO 44 I=ISTR,IEND
      DIFF=D(I)-RINT(I)
      SD=SD+DIFF
      A=ABS(DIFF)
      SUM=SUM+A
      WTAD=WTAD+A/D(I)
      SSQ=SSQ+DIFF*DIFF
      44  CONTINUE
      WRITE(1,302)RES,SD,SUM,SSQ,WTAD
      302  FORMAT(2X,'RESOLUTION= ',F4.2,' CM-1'
      1 /2X,'SUM. OF DIFF.= ',E13.6
      1 /2X,'SUM. OF ABS. DIFF.= ',E13.6
      1 /2X,'SUM. OF SQUARE DIFF.= ',E13.6
      1 /2X,'RELATIVE ABS. DIFF.= ',E13.6)
      CALL EXIT
      END

```

Results of Program CMPR (UT8:31-8:34, March 1, 1975)

TC

.R LOADER
*CMPR1/I/G

TEMPERATURE= 190.0
 INPUT SYNTHETIC DATA FILE= D19030
 ORIGINAL FILE NO. =19
 DATA FILE NAME =D00030
 SUM. OF DIFF.= -0.115395E-03
 SUM. OF ABS. DIFF.= 0.194718E+04
 SUM. OF SQUARE DIFF.= 0.372307E+05
 SUM. OF RELATIVE ABS. DIFF.= 0.707013E+02

.R LOADER
*CMPR1/I/G

TEMPERATURE= 200.0
 INPUT SYNTHETIC DATA FILE= D20030
 ORIGINAL FILE NO. =19
 DATA FILE NAME =D00030
 SUM. OF DIFF.= 0.979900E-04
 SUM. OF ABS. DIFF.= 0.191961E+04
 SUM. OF SQUARE DIFF.= 0.359015E+05
 SUM. OF RELATIVE ABS. DIFF.= 0.389567E+02

.R LOADER
*CMPR1/I/G

TEMPERATURE= 210.0
 INPUT SYNTHETIC DATA FILE= D21030
 ORIGINAL FILE NO. =19
 DATA FILE NAME =D00030
 SUM. OF DIFF.= 0.133038E-03
 SUM. OF ABS. DIFF.= 0.191120E+04
 SUM. OF SQUARE DIFF.= 0.367454E+05
 SUM. OF RELATIVE ABS. DIFF.= 0.380948E+02

.R LOADER
*CMPR1/I/G

TEMPERATURE= 220.0
 INPUT SYNTHETIC DATA FILE= D22030
 ORIGINAL FILE NO. =19
 DATA FILE NAME =D00030
 SUM. OF DIFF.= 0.415444E-03
 SUM. OF ABS. DIFF.= 0.191473E+04
 SUM. OF SQUARE DIFF.= 0.367868E+05
 SUM. OF RELATIVE ABS. DIFF.= 0.377644E+02

.R LOADER
*CHPRI/I/O

TEMPERATURE= 230.0
INPUT SYNTHETIC DATA FILE= D23030
ORIGINAL FILE NO. =19
DATA FILE NAME =D00030
SUM. OF DIFF.= 0.336409E-03
SUM. OF ABS. DIFF.= 0.192361E+04
SUM. OF SQUARE DIFF.= 0.370037E+05
SUM. OF RELATIVE ABS. DIFF.= 0.680347E+02

BEST AVAILABLE COPY

.R LOADER
*CHPRI/I/O

TEMPERATURE= 240.0
INPUT SYNTHETIC DATA FILE= D24030
ORIGINAL FILE NO. =19
DATA FILE NAME =D00030
SUM. OF DIFF.= 0.452280E-03
SUM. OF ABS. DIFF.= 0.193672E+04
SUM. OF SQUARE DIFF.= 0.373769E+05
SUM. OF RELATIVE ABS. DIFF.= 0.687400E+02

APPENDIX E
VALUES OF INSTRUMENTAL RESPONSE

The values in the following table are stored in data filed 'DAIR DA.'
Total number of values is 70. The rest of them are equal to 1.

| No. | Relative Response | No. | Relative Response |
|-----|-------------------|-----|-------------------|
| 1 | 0.715 | 21 | 0.904 |
| 2 | 0.725 | 22 | 0.912 |
| 3 | 0.735 | 23 | 0.920 |
| 4 | 0.748 | 24 | 0.928 |
| 5 | 0.769 | 25 | 0.935 |
| 6 | 0.771 | 26 | 0.942 |
| 7 | 0.781 | 27 | 0.949 |
| 8 | 0.790 | 28 | 0.956 |
| 9 | 0.801 | 29 | 0.962 |
| 10 | 0.810 | 30 | 0.969 |
| 11 | 0.820 | 31 | 0.974 |
| 12 | 0.830 | 32 | 0.978 |
| 13 | 0.840 | 33 | 0.982 |
| 14 | 0.849 | 34 | 0.985 |
| 15 | 0.857 | 35 | 0.988 |
| 16 | 0.868 | 36 | 0.991 |
| 17 | 0.874 | 37 | 0.994 |
| 18 | 0.881 | 38 | 0.996 |
| 19 | 0.889 | 39 | 0.998 |
| 20 | 0.896 | 40 | 0.999 |

APPENDIX F

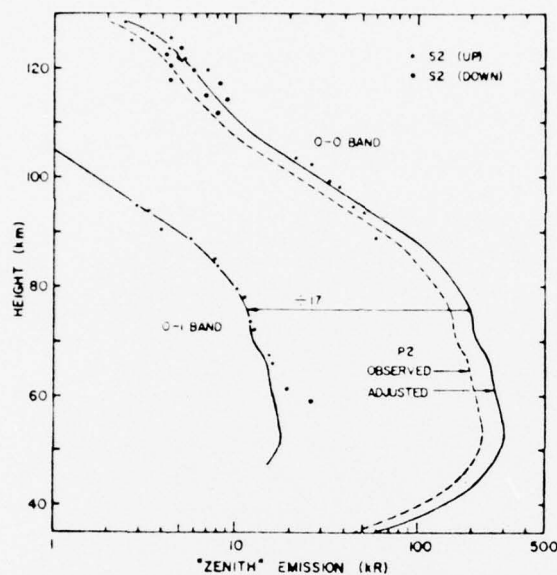


Figure F.1. The observation of zenith emission of $O_2(b^1\Sigma_g^+)$ of atmospheric (0,1) band from rocket; the points refer to spectrometer, and the dash line refers to photometer. The solid line is the adjusted curve to make the intensities agree. [Wallace and Hunt, 1968].

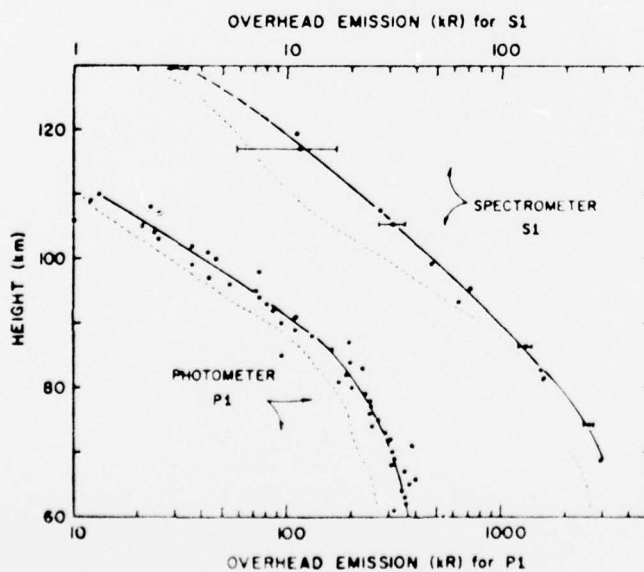


Figure F.2. Zenith emission rates observed by photometer P_1 and spectrometer S_1 . [Wallace and Hunt, 1968].

APPENDIX G

Measured Spectrum of $O_2(b^1\Sigma_g^+)$ atmospheric (0,1) band.

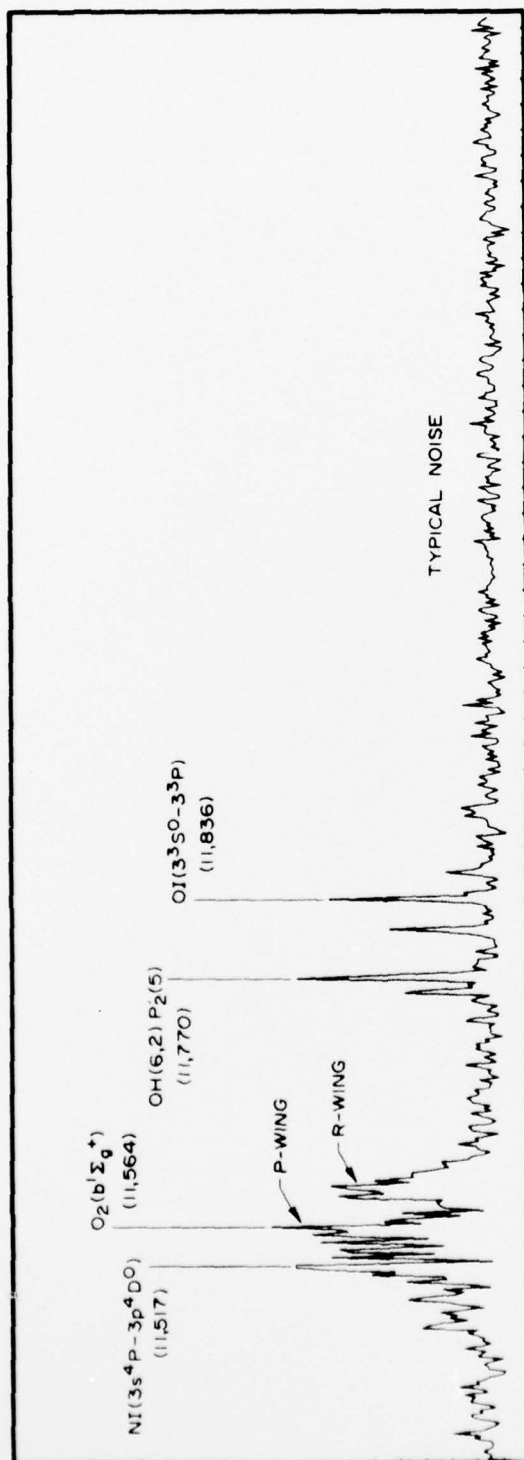


Figure G.1. Coadded (7) spectrum of $O_2(b^1\Sigma_g^+)$ atmospheric (0,1) band obtained from zenith observations at Poker Flat, Alaska, at 0831-0834 hrs. UT, on March 1, 1975. (Feature wavenumbers are given in cm^{-1}).

APPENDIX H
DISTRIBUTION LIST

Department of Defense

Director
Defense Advanced Rsch Proj Agency
Architect Building
1400 Wilson Blvd.
Arlington, VA 22209

01CY Attn: LTC W. A. Whitaker
01CY Attn: STO Capt J. Justice
01CY Attn: Major Gregory Canavan

Defense Documentation Center
Cameron Station
Alexandria, Va 22314

(12 copies if open publication,
otherwise 02 CY)

12CY Attn: TC

Director
Defense Nuclear Agency
Washington, D.C. 20305

03CY Attn: STTL Tech Library
01CY Attn: STSI Archives
03CY Attn: RAAE Charles A. Blank
01CY Attn: RAAE Harold C. Fitz, Jr.
01CY Attn: RAAE Maj John Clark

Dir. of Defense Rsch & Engineering
Department of Defense
Washington D.C. 20301

01CY Attn: DD/S&SS Daniel Brockway
01CY Attn: DD/S&SS Richard S.
Ruffine

Commander
Field Command
Defense Nuclear Agency
Kirtland AFB, NM 84115

01CY Attn: FCPR

Chief
Livermore Division FLD Command DNA
Lawrence Livermore Laboratory
P. O. Box 808
Livermore, CA 94550

01CY Attn: FCPRL

Department of Army

Commander/Director
Atmospheric Sciences Laboratory
U.S. Army Electronics Command
White Sands Missile Range, NM 88002

01CY Attn: DRSEL-BL-SY-S
F. E. Niles
01CY Attn: E. Butterfield
DRSEL-BL-SY-R

Commander
Harry Diamond Laboratories
2800 Powder Mill Road
Adelphi, MD 20783

(CNWDI-Inner Envelope: Attn:
DRXDO-RBH)

02CY Attn: DRXDO-NP

Commander
U.S. Army Nuclear Agency
Fort Bliss, TX 79916

01CY Attn: ATCA-NAW J. Berberet

Department of Navy

Chief of Naval Research
Navy Department
Arlington, VA 22217

01CY Attn: Code 427 CDR
Ronald J. Oberle

Commander
Naval Electronics Laboratory Center
San Diego, CA 92152

01CY Attn: Code 2200 1 Verne E.
Hilderbrand
01CY Attn: Code 2200 11an
Rothmuller

Director
Naval Research Laboratory
Washington, D.C. 20375

01CY Attn: Douglas P. McNutt
01CY Attn: Code 7127
Charles Y. Johnson
01CY Attn: Code 2027 Tech Lib
01CY Attn: Code 7700
Timothy P. Coffey
01CY Attn: Code 7701
Jack D. Brown
01CY Attn: 7750
Darrell F. Strobel
01CY Attn: Code 7750
Paul Julienne

Commander
Naval Surface Weapons Center
White Oak, Silver Spring, MD 20910

01CY Attn: Code WA501
Navy Nuc Prgms Off

Department of the Air Force

AF Geophysics Laboratory, AFSC
Hanscom AFB, MA 01731

01CY Attn: LKB Kenneth S.W. Champion
01CY Attn: OP John S. Garing
01CY Attn: OPR Alva T. Stair

AF Weapons Laboratory, AFSC
Kirtland AFB, NM 87117

01CY Attn: DYT Capt David W. Goetz
01CY Attn: SUL
01CY Attn: DYT LTC Don Mitchell

Commander
ASD
WPAFB, OH 45433

01CY Attn: ASD-YH-EX
LTC Robert Leverette

SAMSO/SZ
Post Office Box 92960
Worldway Postal Center
Los Angeles, CA 90009
(Space Defense Systems)

01CY Attn: SZJ Maj Lawrence Doan

U.S. Energy Rsch and Dev Admin

Division of Military Application
U.S. Energy Rsch & Dev Admin
Washington, D.C. 20545

01CY Attn: Doc Con for
Maj. D.A. Haycock

Los Alamos Scientific Laboratory
P.O. Box 1663
Los Alamos, NM 87545

01CY Attn: Doc Con for
R.A. Jeffries

Other Government

Department of Commerce
Office of Telecommunications
Institute for Telecom Science
Boulder, CO 80302

01CY Attn: William F. Utlaut
01CY Attn: Glenn Falcon

Department of Defense Contractor

Aerodyne Research, Inc.
Bedford Research Park
Crosby Drive
Bedford, MA 01730

01CY Attn: F. Bien
01CY Attn: M. Camac

Aerospace Corporation
P.O. Box 92957
Los Angeles, CA 90009

01CY Attn: T. Taylor
01CY Attn: R. Grove
01CY Attn: R.D. Rawcliffe
01CY Attn: Harris Mayer

Denver, University of
Colorado Seminary
Denver Research Institute
P.O. Box 10127
Denver, CO 80210

(Only 1 copy of Class Rpts)
01CY Attn: Sec Officer for
Mr. Van ZYL
01CY Attn: Sec Officer for
David Murcray

General Electric Company
Tempo-Center for Advanced Studies
816 State Street (P.O. Drawer QQ)
Santa Barbara, CA 93102

05CY Attn: Dasiac Art Feryok
01CY Attn: Warren S. Knapp

General Research Corporation
P.O. Box 3587
Santa Barbara, CA 93105

01CY Attn: John Ise, Jr.

Geophysical Institute
University of Alaska
Fairbanks, AK 99701
(All Class Attn: Security Officer)

01CY Attn: T. N. Davis
(Uncl. only)
03CY Attn: Neal Brown
(Uncl. only)

Honeywell Incorporated
Radiation Center
2 Forbes Road
Lexington, MA 02173

01CY Attn: W. Williamson

Institute for Defense Analyses
400 Army-Navy Drive
Arlington, VA 22202

01CY Attn: Ernest Bauer
01CY Attn: Hans Wolfhard

Lockheed Missiles and Space Company
3251 Hanover Street
Palo Alto, CA 94304

01CY Attn: John B. Cladis
Dept. 52-12
01CY Attn: J. B. Reagan
D/52-12
01CY Attn: Billy M. McCormac
Dept. 52-54
01CY Attn: Tom James
01CY Attn: Robert D. Sears
Dep. 52-14
01CY Attn: John Kumer
01CY Attn: Martin Walt Dpt. 52-10
01CY Attn: Richard G. Johnson
Dept. 52-12

Mission Research Corporation
735 State Street
Santa Barbara, CA 93101

01CY Attn: P. Fischer
01CY Attn: D. Archer

Photometrics, Inc.
442 Marrett Road
Lexington, MA 02173

01CY Attn: Irving L. Kofsky

Physical Dynamics Inc.
P.O. Box 1069
Berkeley, CA 94701

01CY Attn: Joseph B. Workman

Physical Sciencer, Inc.
30 Commerce Way
Woburn, MA 01801

01CY Attn: Kurt Wray

R & D Associates
P.O. Box 9695
Marina Del Rey, CA 90291

01CY Attn: Forrest Gilmore
01CY Attn: Robert E. Lelevier

R & D Associates
1815 N. Ft. Myer Drive
11th Floor
Arlington, VA 22209

01CY Attn: Herbert J. Mitchell

The Rand Corporation
1700 Main Street
Santa Monica, CA 90406

01CY Attn: James Oakley

Science Applications, Inc.
P.O. Box 2351
La Jolla, CA 92038

01CY Attn: Daniel A. Hamlin

H-4

Space Data Corporation
1331 South 26th Street
Phoenix, AZ 85034

01CY Attn: Edward F. Allen

Stanford Research Institute
333 Ravenswood Avenue
Menlo Park, CA 94025

01CY Attn: Walter G. Chestnut
01CY Attn: M. Baron
01CY Attn: Ray L. Leadabrand

Stanford Research Institute
1611 North Kent Street
Arlington, VA 22209

01CY Attn: Warren W. Berning

Technology International Corporation
75 Wiggins Avenue
Bedford, MA 01730

01CY Attn: W. P. Boquist

Utah State University
Logan, UT 84322

01CY Attn: Doran Baker
01CY Attn: Kay Baker
01CY Attn: D. Burt
01CY Attn: C. Wyatt

Visidyne, Inc.
19 Third Avenue
North West Industrial Park
Burlington, MA 01803

01CY Attn: William Reidy
01CY Attn: J. W. Carpenter
01CY Attn: T. C. Degges